



# 1 **Characterizing Southeast Greenland fjord surface ice and** 2 **freshwater flux to support biological applications**

3  
4 Twila A. Moon<sup>1\*</sup>, Benjamin Cohen<sup>2\*</sup>, Taryn E. Black<sup>2,3</sup>, Kristin L. Laidre<sup>2</sup>, Harry Stern<sup>2</sup>, Ian Joughin<sup>2</sup>

5 <sup>1</sup>National Snow and Ice Data Center, Cooperative Institute for Research in Environmental Sciences, University of Colorado,  
6 Boulder, 80309, USA

7 <sup>2</sup>Polar Science Center, Applied Physics Laboratory, University of Washington, Seattle, 98105, USA

8 <sup>3</sup>Earth System Science Interdisciplinary Center, University of Maryland, College Park, MD 20742, USA

9 \* These authors contributed equally to the work.

10 *Correspondence to:* Twila A. Moon (twila.moon@colorado.edu)

## 11 **Short summary. (500-character limit)**

12 The complex geomorphology of Southeast Greenland (SEG) creates dynamic fjord habitats for marine top predators, with  
13 glacier-derived floating ice, pack and landfast sea ice, and freshwater flux. We investigate the SEG fjord physical  
14 environment, with focus on surface ice conditions, to provide a regional characterization to support biological research. As  
15 Arctic warming continues, SEG may serve as a long-term refugia for ice-dependent wildlife due to projected regional ice  
16 sheet persistence.

## 18 **Abstract.**

19 Southeast Greenland (SEG) is characterized by complex morphology and environmental processes that create dynamic  
20 habitats for resident marine top predators. Active glaciers producing solid ice discharge, freshwater flux, offshore sea ice  
21 transport, and seasonal landfast ice formation all contribute to a variable, transient environment within SEG fjord systems.  
22 Here, we investigate a selection of physical processes in SEG to provide a regional characterization to reveal physical system  
23 processes and support biological research. SEG fjords exhibit high fjord-to-fjord variability regarding bathymetry, size,  
24 shape, and glacial setting, influencing some processes more than others. For example, the timing of offshore sea ice  
25 formation in fall near SEG fjords progresses temporally southward across latitudes while the timing of offshore sea ice  
26 disappearance is less dependent on latitude. Rates of annual freshwater flux into fjords, in contrast, are highly variable across  
27 SEG, with annual average input values ranging from  $\sim 1 \times 10^8 \text{ m}^3$  to  $\sim 1.25 \times 10^{10} \text{ m}^3$  ( $\sim 0.1$ – $12.5 \text{ Gt}$ ) for individual fjords.  
28 Similarly, rates of solid ice discharge in SEG fjords vary widely – in part due to the irregular distribution of active glaciers  
29 across the study area ( $60^\circ\text{N}$ – $70^\circ\text{N}$ ). Landfast sea ice, assessed for 8 focus fjords, is seasonal and has a spatial distribution  
30 highly dependent on individual fjord topography. Conversely, glacial ice is deposited into fjord systems year-round, with the



31 spatial distribution of glacier-derived ice dependent on glacier termini location. As climate change continues to affect SEG,  
32 the evolution of these metrics will be individually variable in their response, and next steps should include moving from  
33 characterization to system projection. Due to projected regional ice sheet persistence that will continue to feed glacial ice  
34 into fjords, it is possible that SEG could remain a long-term (century to millennia scale) refugia location for polar bears and  
35 other ice-dependent species, demonstrating a need for continued research on the SEG physical environment.

## 36 **1 Introduction and motivation**

37 Rapid changes across the Greenland coastal environment are influencing the linked physical and biological fjord systems.  
38 The Greenland Ice Sheet and peripheral glaciers and ice caps are undergoing substantial retreat along marine- and land-  
39 terminating boundaries, revealing new ocean and terrestrial zones (Moon et al., 2020; Kochtitzky and Copland, 2022;  
40 Bosson et al., 2023). For some marine-terminating glaciers, changing ice dynamic and terminus locations are altering iceberg  
41 calving styles or rates (e.g., van Dongen et al., 2021), with potential influence on glacier-derived fjord ice that forms  
42 important habitat for polar bears (*Ursus maritimus*), seals, and many other marine species (e.g., Laidre et al., 2022).  
43 Increases in ice sheet surface melt are also changing the timing and quantity of subglacial meltwater discharge and terrestrial  
44 riverine freshwater input into the coastal fjords (e.g., van As et al., 2018). Depending on the fjord bathymetry and glacier  
45 grounding line depth, this subglacial discharge may entrain deeper nutrient-rich ocean water and assist in redistributing it to  
46 the surface photic zone to support enhanced productivity (Hopwood et al., 2018; Meire et al., 2023) or alter the ecosystem in  
47 other potentially significant ways (e.g., Hawkings et al., 2021; Hopwood et al., 2020). Additional terrestrial runoff adds to  
48 coastal zone freshwater (e.g., from Norway: McGovern et al., 2020), though impacts are less well documented for Greenland  
49 (Meire et al., 2023). Despite the rapid changes underway, progress is still needed on fundamental physical characterization  
50 of the Greenland coastal zone, including the remote Southeast Greenland (SEG) region (Fig. 1).

51 Earlier work characterized the landfast sea ice and glacier-derived fjord surface ice for five SEG fjords that were biologically  
52 relevant to polar bears (Laidre et al., 2022). This research revealed that glacier-derived fjord surface ice exists during time  
53 periods outside of the landfast sea ice season, and that this glacier-derived ice can act as an alternative habitat platform for  
54 marine species, allowing small populations to persist in areas they may not otherwise be able to. Motivated by the biological  
55 insight enabled via enhanced physical system knowledge, here we extend our characterization of the SEG fjord physical  
56 environment. Examining the full SEG region of interest (Fig. 1), we describe the freshwater flux, offshore sea ice, and solid  
57 glacier ice discharge behavior across the region during 2015 through 2019. We also expand from the five focus fjords used  
58 in Laidre et al. (2022) to eight focus fjords across SEG (Fig. 1, Table 1). For these focus fjords, we analyze landfast sea ice  
59 and glacier-derived ice presence in time and space and compare these results with offshore sea ice from satellite

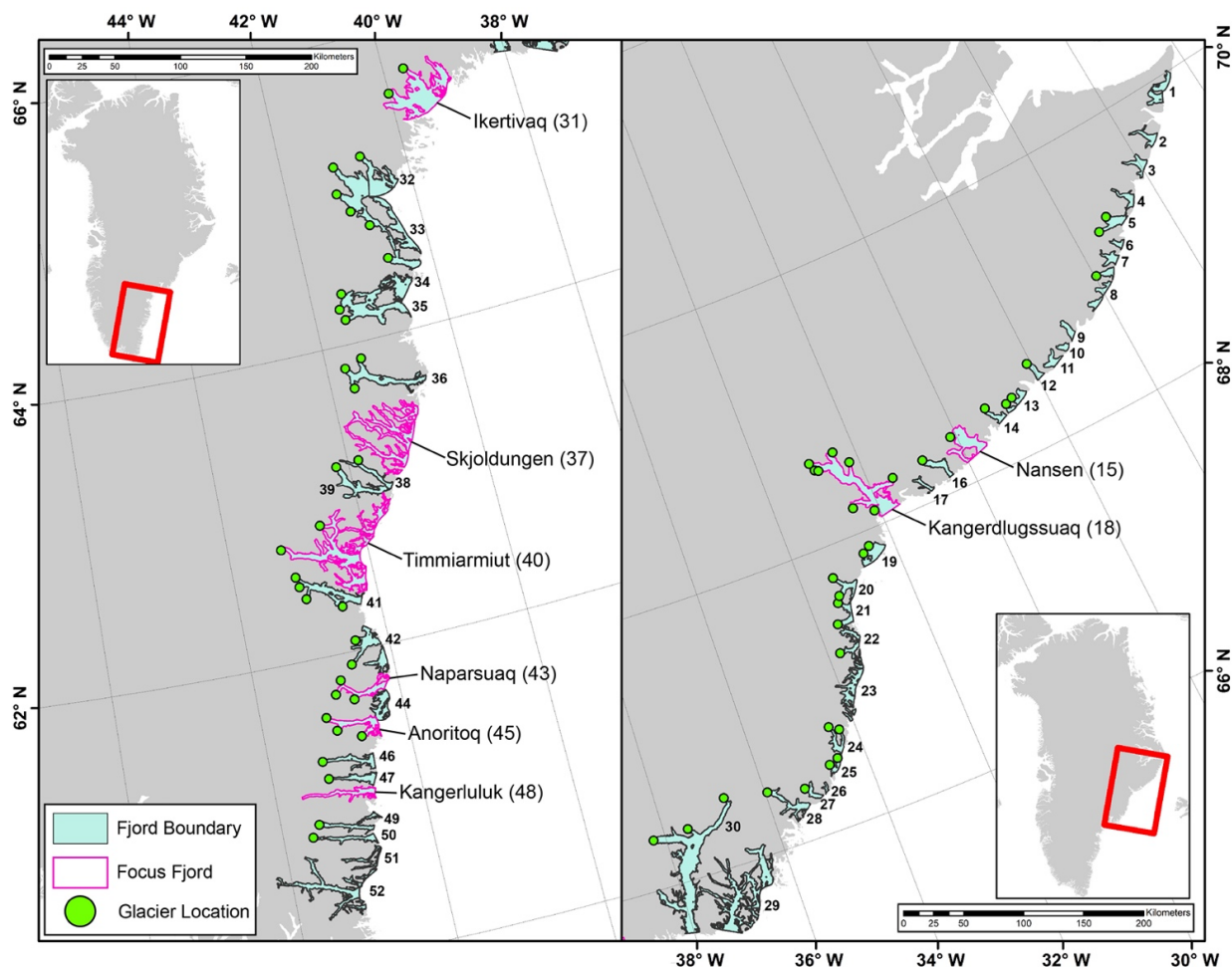


**Figure 1. Southeast Greenland region of study, showing the 52 fjord systems defined across the full region (blue shading) and the 8 focus fjords used for fast ice and glacier-derived ice analysis (pink outlines). Locations of outlet glaciers considered in analysis of solid ice discharge are shown (green points).**

60 observations, and freshwater flux, sea surface temperature, and sea ice cover from a regional climate model. Our results are  
61 designed to expand knowledge of SEG fjord environments and pair with ongoing and future research into the linked physical  
62 and biological systems of the region.

## 63 **2 Southeast Greenland (SEG) study region**

64 While some fjords, for example Sermilik on the East Coast and Nuup Kangerlua (previously also known as Godthåbsfjord)  
65 on the West Coast, have been studied more extensively, many Greenland fjords have proven difficult to study, including in  
66 Southeast Greenland (SEG). Here, we define the SEG region of interest as extending from 60° N to 70° N (Fig. 1). This



67 region is of particular interest for a variety of reasons. First, it provides habitat for a genetically distinct polar bear  
68 subpopulation only recently identified (Laidre et al., 2022). Second, it contains particularly remote regions of Greenland  
69 coastline, far from any human settlements and difficult to access for research. Third, it is an area of very high winter  
70 precipitation (Gallagher et al., 2021) and modeling work indicates that it may be one of the last regions of Greenland to  
71 retain substantial coastal land ice (Aschwanden et al., 2019; Bochow et al., 2023). Fourth, it is a region of rapid change, not  
72 only in documented changes to the coastal glaciers and ice sheet (Moon et al., 2020) but also notable declines in offshore sea  
73 ice and warming of coastal ocean currents (Heide-Jørgensen et al., 2022).

### 74 **3 Data and methods**

75 In this study, the fjords in SEG are numbered 1-52 going from north to south (Fig. 1). We also use our own digitized fjord  
76 boundaries created based on synthetic aperture radar (SAR) image mosaics (Cohen et al., 2023; see Code and data availability).  
77 Our analysis is focused on 1 January 2015 through 31 December 2019 to align with SEG polar bear data collection and the  
78 time period of interest established by Laidre et al. (2022).

79 To characterize a range of environmental metrics, we take advantage of existing data products, such as freshwater flux, iceberg  
80 discharge, and regional climate model output, to create new datasets that support SEG-wide analysis. While remote sensing is  
81 necessary to characterize a region of this scale, the spatial resolution needed (10s to 100s of meters) for some data types is  
82 difficult to achieve from many standard remote sensing products, such as sea-ice cover data products (often with multi-  
83 kilometer resolution). Though researchers are working towards automated classification schemes at the spatial scales needed  
84 for this type of analysis (e.g., Scheick et al., 2019; Soldal et al. 2019), we are unaware of any that can support our specific  
85 study needs. We therefore undertook extensive manual digitization to create landfast sea ice and glacier-derived fjord ice data  
86 records. Along with supporting our analysis, these data (Cohen et al., 2023) should be helpful for ongoing work to improve  
87 machine learning techniques for classifying fjord environments.

88 Due to the effort required to create manually digitized datasets, we selected eight focus fjords for landfast sea ice and glacier-  
89 derived fjord ice analysis (Fig. 1, Table 1). Our focus fjords include five that were selected for Laidre et al. (2022): Skjoldungen  
90 (63.3° N), Timmiarmiut (62.6° N), Naparsuaq (61.7° N), Anoritoq (61.5° N), and Kangerluluk (61.1° N). These fjords have  
91 been occupied by polar bears for multiple years based on telemetry data collected since 2015 and comprised the core range of  
92 the SEG polar bear population. Here, we expand the fjord selection to include three more northerly focus fjords: Ikertivaq  
93 (65.4° N), Kangerdlugssuaq (68.1° N), and Nansen (68.2° N). Ikertivaq and Kangerdlugssuaq fjords are heavily used by polar  
94 bears that inhabit Northeast Greenland, while their presence was scarcer in Nansen during 2015–2019. The map-view  
95 geometries of our focus fjords (Fig. 1) cover a wide range, from relatively simply shaped long, narrow fjords (e.g., fjords 43  
96 and 48) to complex interconnected channel systems (e.g., fjords 37 and 40).



**Table 1. Focus fjord spatial information, including fjord reference names, areas (km<sup>2</sup>), and bounding coordinates used for analysis.**

Fjord Name & Number	Analysis area (km <sup>2</sup> )	Top Right (lat, lon)	Bottom Left (lat, lon)
Nansen (15)	375	(68.43, -29.51)	(68.16, -30.32)
Kangerdlugssuaq (18)	880	(68.64, -31.52)	(68.05, -32.98)
Ikertivaq (31)	894	(65.74, -38.96)	(65.36, -40.13)
Skjoldungen (37)	793	(63.57, -40.80)	(63.08, -41.94)
Timmiarmiut (40)	1079	(62.98, -41.52)	(62.37, -43.22)
Naparsuaq (43)	182	(61.83, -42.11)	(61.68, -42.90)
Anoritoq (45)	217	(61.61, -42.40)	(61.41, -43.12)
Kangerluluk (48)	184	(61.12, -42.64)	(61.02, -43.64)

### 97 3.1 Solid ice discharge across SEG

98 To compute solid-ice discharge from 2015 through 2019, we used data derived from glacier gates (Mankoff et al., 2020b;  
99 Mankoff et al., 2020c). These data were used to create individual glacier discharge time series as well as discharge by-fjord,  
100 including daily, monthly, annual and season mean, and cumulative 2015-2019 discharge records (Cohen et al., 2023).  
101 Beginning with a glacier dataset evolved from Moon et al. (2020), we manually associated each of these glaciers (shown in  
102 Fig. 1) with a glacier gate in the Mankoff et al. (2020b) solid ice discharge dataset; in some cases, there were multiple gates  
103 corresponding to a single glacier, and we summed the discharge from these gates accordingly. We filtered out data at times  
104 when the dataset coverage attribute was less than 50% (Mankoff et al., 2020b). We also note that some glaciers apparent in  
105 satellite imagery are not included in either the Moon et al. (2020) or Mankoff et al. (2020b) datasets (usually because they  
106 are narrow and/or slow moving) and are therefore not included in our solid ice discharge results, even though glacier-derived  
107 ice in fjords is recorded in a separate dataset (section 3.5).

108 Solid ice discharge is interpolated for individual glaciers between the first and last dates with observed discharge to create  
109 daily time series. We linearly interpolate between observed discharge values to fill data gaps and use the observed discharge  
110 and error to calculate the interpolation error (Eqn 15, White, 2017). At the fjord level, the interpolated daily discharge time  
111 series for each glacier are summed together, and the fjord discharge error is the root of the sum of the squares of the glacier



112 discharge errors. The daily time series is then used to construct other solid ice discharge metrics, including a monthly time  
113 series, as displayed in Fig. 9d.

114 The interpolation procedure, combined with differences in the observational discharge time series length for each glacier,  
115 introduces a small discrepancy between the cumulative discharge from all glaciers and the cumulative discharge from all  
116 fjords (~21 Gt or ~2%). Essentially, the first and last valid dates in the observational time series vary for each glacier, and  
117 interpolation preserves the first and last dates in each discharge time series. Of the 67 glaciers with observed discharge, the  
118 interpolated time series include discharge data starting from 1 January 2015 for 31 glaciers, and ending on or after 26  
119 December 2019 for 65 glaciers. While the glaciers with gaps at the beginning or end of their records were likely discharging,  
120 discharge observations were absent or filtered out for quality, and so the first or last several days in the interpolated time  
121 series for those glaciers are empty. Consequently, of the 33 fjords with observed discharge from at least one glacier, 11  
122 fjords have discharge time series starting from 1 January 2015, and 31 end on 26 December 2019. This results in a slightly  
123 lower cumulative discharge for a fjord than for its component glaciers because fjord discharge is not computed on a date  
124 when any glacier in the fjord has no discharge value. We chose to accept this small discrepancy since it does not impact our  
125 conclusions.

### 126 **3.2 Freshwater flux across SEG**

127 To compute daily time series of freshwater discharge into each fjord from 2015 through 2019, we used freshwater discharge  
128 data, including surface runoff and subglacial discharge, from Greenland land and ice basins (Mankoff, 2020; Mankoff et al.,  
129 2020a). The freshwater discharge data products are created by applying a flow routing algorithm to digital elevation models  
130 of the land and ice sheet surfaces and the ice sheet bed to identify land surface and subglacial streams, stream outlets, and  
131 basins upstream of those outlets. Subsequently, daily runoff from a regional climate model is summed over each of the  
132 identified basins, and instantaneously routed to the appropriate basin outlets. We calculated freshwater discharge into our  
133 fjords by using the command line tool provided with Mankoff et al. (2020a) to identify all outlets within a 500 m buffer of  
134 each fjord boundary; we applied this buffer to account for differences in coastline data products and to ensure that we  
135 captured all freshwater discharge outlets. We then used the command line tool to compute daily freshwater discharge  
136 originating from their predefined land and ice basins and going through the outlets that we identified and into each of our  
137 fjord basins. We used discharge values from both the Modèle Atmosphérique Régional (MAR: Fettweis et al. 2017) and the  
138 Regional Atmospheric Climate Model (RACMO: Noël et al., 2019), both of which were statistically downscaled to a  
139 common 1 km grid and archived for use with these freshwater discharge tools (Mankoff, 2020); we used version 4.2 of the  
140 archival data. Due to a longer time series and to align with other sampled metrics, we relied primarily on the MAR time  
141 series, but we have included the RACMO discharge output in our own archival data.



142 We also analyzed freshwater discharge variations with depth, including terrestrial runoff and subglacial discharge. We used  
143 the same command line interface and source data (Mankoff et al., 2020a) to identify all freshwater discharge outlets within  
144 each buffered fjord boundaries. These outlet output data include outlet elevation above or below sea level. For outlets above  
145 sea level, we clipped their elevation values to 0 m under the assumption that water flowing from these outlets enters the  
146 fjords at sea level (i.e., surface runoff). Using these data, we calculated daily time series of total freshwater discharge, binned  
147 by discharge depth, for each fjord (for example, Fig. 9c).

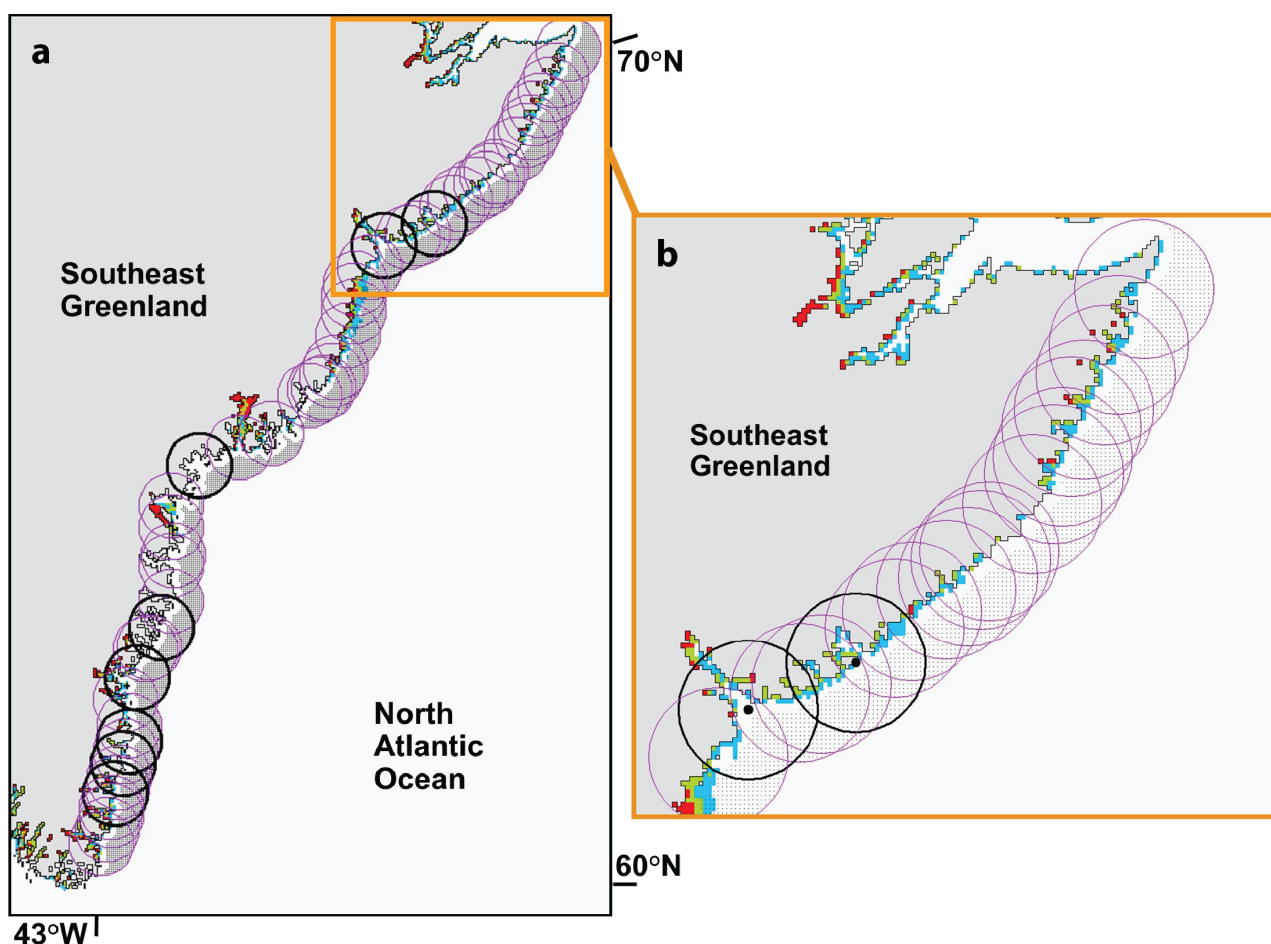


Figure 2. Regions at the mouths of (a) fjords 1-52 and (b) fjords 1-19 (circles of radius 50 km) for offshore sea-ice analysis. Small black dots indicate locations of gridded sea-ice concentration data from AMSR2. Grid cell size is approximately  $3.125 \times 3.125$  km. A buffer zone of three grid cells from land is excluded from analysis due to land contamination of the ocean data, which can be seen in the form of spurious sea ice (red, green, and blue cells) for this date of October 2, 2013, when sea ice is almost surely not present along this portion of the coast. The black circles are associated with the focus fjords of this study.



### 148 **3.3 Sea ice and sea surface temperature**

149 To characterize the offshore sea ice at the mouths of the fjords, we used sea-ice concentration data derived from the passive  
150 microwave AMSR2 (Advanced Microwave Scanning Radiometer 2) instrument onboard the GCOM-W satellite operated by  
151 the Japan Aerospace Exploration Agency (Kaleschke and Tian-Kunze, 2016). The brightness temperature data were  
152 processed at the University of Hamburg using the ASI algorithm (Beitsch et al., 2014) to create daily gridded fields of sea-  
153 ice concentration with nominal grid cell size  $3.125 \times 3.125$  km. We defined circles of radius 50 km centered at the mouths of  
154 the fjords (Fig. 2a). Within each circle we identified the offshore grid cells, excluding a buffer zone of three grid cells from  
155 land because the sea-ice signal in those cells may be contaminated by the signal from land (Fig. 2b). We then calculated the  
156 daily sea-ice area for the valid grid cells within each circle during 2015-2019. Figure 9a shows an example, in which the  
157 black curve is the daily sea-ice area, and the purple curve is a 31-day running mean. We defined a threshold equal to 15% of  
158 the mean March-April sea-ice area (horizontal black dotted line) and found the dates each year when the 31-day running  
159 mean crossed the threshold (vertical yellow dashed lines). The date in the spring when the sea-ice area drops below the  
160 threshold on its way to the summer minimum is called the spring transition date; the date in the fall when the sea-ice area  
161 climbs above the threshold on its way to the winter maximum is called the fall transition date. The transition dates for all  
162 fjords and all years are shown in Fig. 6.

163 To include further comparison metrics for sea ice coverage and also sea surface temperatures at the fjord mouth, we sampled  
164 output from MARv3.12 (Fettweis et al. 2017). MAR results have a grid resolution of 6.5 km, and we sample a single grid  
165 cell centered at the fjord mouth, which we extract based on fjord mouth outlines created as a subset of developing the SEG  
166 fjord boundaries (e.g., Fig. 1; Cohen et al., 2023). The FRA variable identifies the open water and sea ice cover percentages,  
167 while the ST2 variable provides the sea surface temperature (SST) for open water and sea ice surface temperature. These are  
168 used together to determine the percent sea ice cover and the SST for the open water fraction. MAR has a hard-coded  
169 maximum sea ice cover of 95%, which we retain in our plotted results (e.g., Fig. 9e). Note that MAR assimilates SST and  
170 sea ice cover data from ERA5 available at a resolution of  $0.3 \times 0.3^\circ$  (Hersbach et al. 2020).

### 171 **3.4 Landfast sea ice for 8 focus fjords**

172 To analyze landfast sea ice, we combined data extracted from imagery via the Operational Land Imager (OLI) onboard the  
173 USGS Landsat 8 satellite with data extracted from images captured by the Moderate Resolution Imaging Spectroradiometer  
174 (MODIS) instruments aboard the NASA Aqua and Terra satellites. There are notable differences between the two datasets:  
175 Landsat 8 imagery provides higher spatial resolution (30 m) with lower temporal resolution (16-day repeat cycle for each  
176 image footprint), while MODIS has lower spatial resolution (250 m) but higher temporal resolution (daily). Clouds and polar  
177 night limit the functional temporal resolution of both Landsat 8 and MODIS as the two satellites operate using optical  
178 sensors..



179 The suitability of every image from 1 January 2015 through 31 December 2019 in the region of interest was manually  
180 inspected for use in our analysis. MODIS imagery was obtained from the NASA Worldview website  
181 (<https://worldview.earthdata.nasa.gov>) and we downloaded the Corrected Reflectance (True Color) images that were  
182 determined to be cloud-free (Fig. 3a). We used the USGS EarthExplorer web tool (<https://earthexplorer.usgs.gov>) to preview  
183 all available Landsat 8 imagery and evaluate cloud cover (with a starting filter of 90% cloud cover). We downloaded cloud-  
184 free Collection 1, Level 1 data (Fig. 3a) and we created multi-band natural color images using bands 4, 3, and 2. We used  
185 both the R “stack” tool included in the “raster” package (<https://cran.r-project.org/web/packages/raster/raster.pdf>) and the  
186 Composite Bands (Data Management) tool in ArcGIS to produce these composites. These composite imagery datasets were  
187 catalogued and served as the foundation for further analysis.

188 Glacial ice, landfast ice, and pack ice share similar visual characteristics and are often adjacent to or intermixed with one  
189 another within SEG fjords. Larger fjord systems, where active glaciers introduce glacial ice and large fjord mouths facilitate  
190 the accretion of pack ice inside the fjords during the frozen season, are especially likely to contain a mixture of ice types.  
191 This is compounded by the intricate geometry of these fjord systems, in which narrow corridors or tortuous coastlines entrap  
192 ice of various types. Thus, we worked to distinguish landfast ice from glacier-derived ice, open water, and pack ice floes  
193 (Fig. 4). By having one person complete the entirety of the digitization process, we attempted to reduce the potential  
194 sensitivity of our manual analysis procedure.

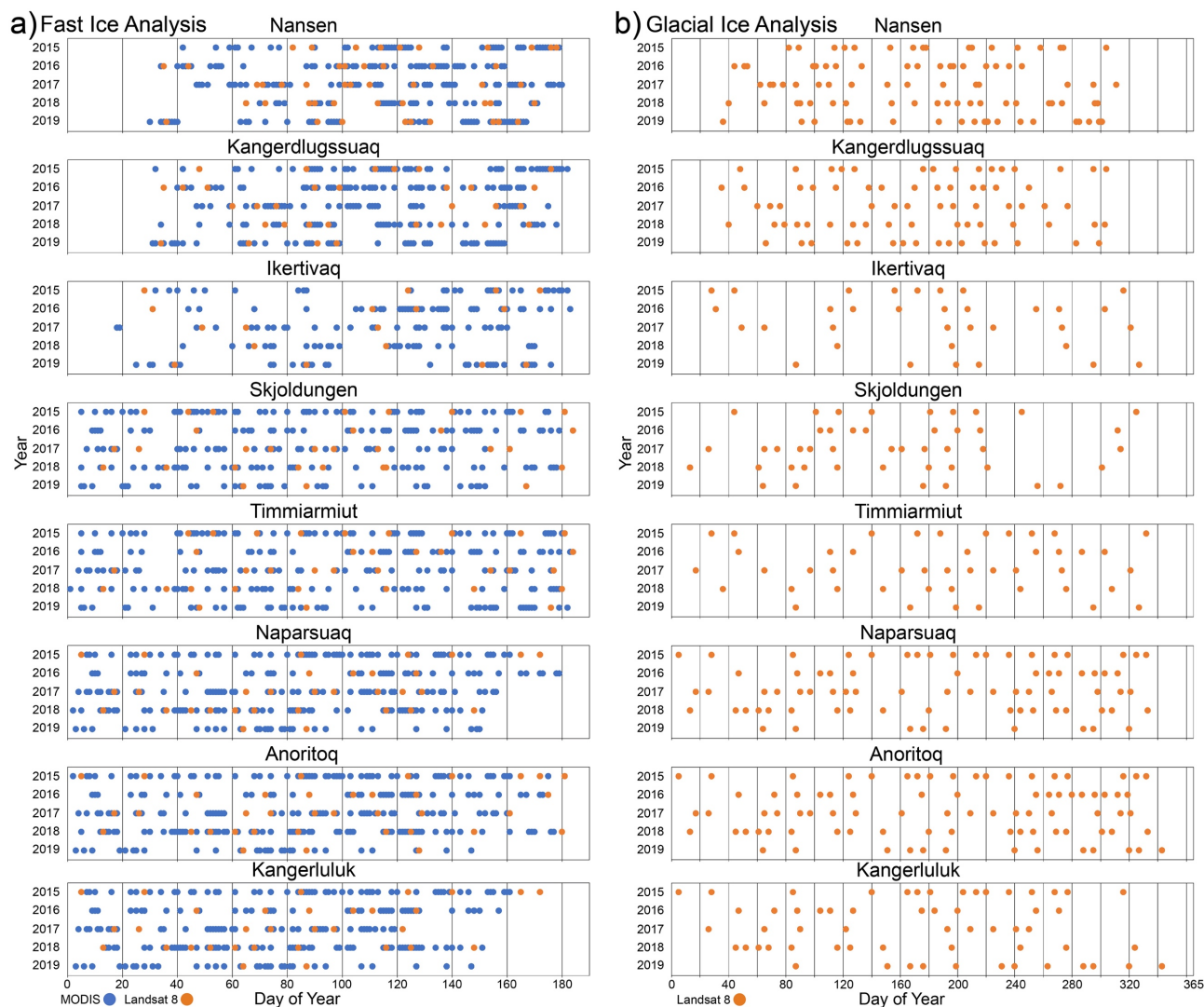


**Figure 3. Data availability during 2015-2019 for a) fast ice analysis from MODIS and Landsat 8 images covering day 0-180 and b) glacial ice analysis from Landsat 8 images covering the full year.**

195 Several visible characteristics in Landsat 8 imagery facilitated the identification of landfast ice: a smooth surface texture  
 196 (especially relative to glacier-derived ice); bright surface character; image-to-image persistence; and adhesion to coastal  
 197 boundaries. Landfast ice is more challenging to distinguish in lower-resolution MODIS imagery. Regarding identification of  
 198 landfast ice in MODIS images, pixel color was the most useful identifier along with image-to-image persistence. Several  
 199 smaller regions in our study area were poorly resolved by MODIS imagery, resulting in varying optical properties (e.g.,  
 200 color, saturation, brightness) for otherwise consistent ice surface characteristics. To address this issue, the higher-resolution  
 201 Landsat 8 imagery was analyzed first and produced landfast-ice boundaries with a higher level of accuracy on the dates when

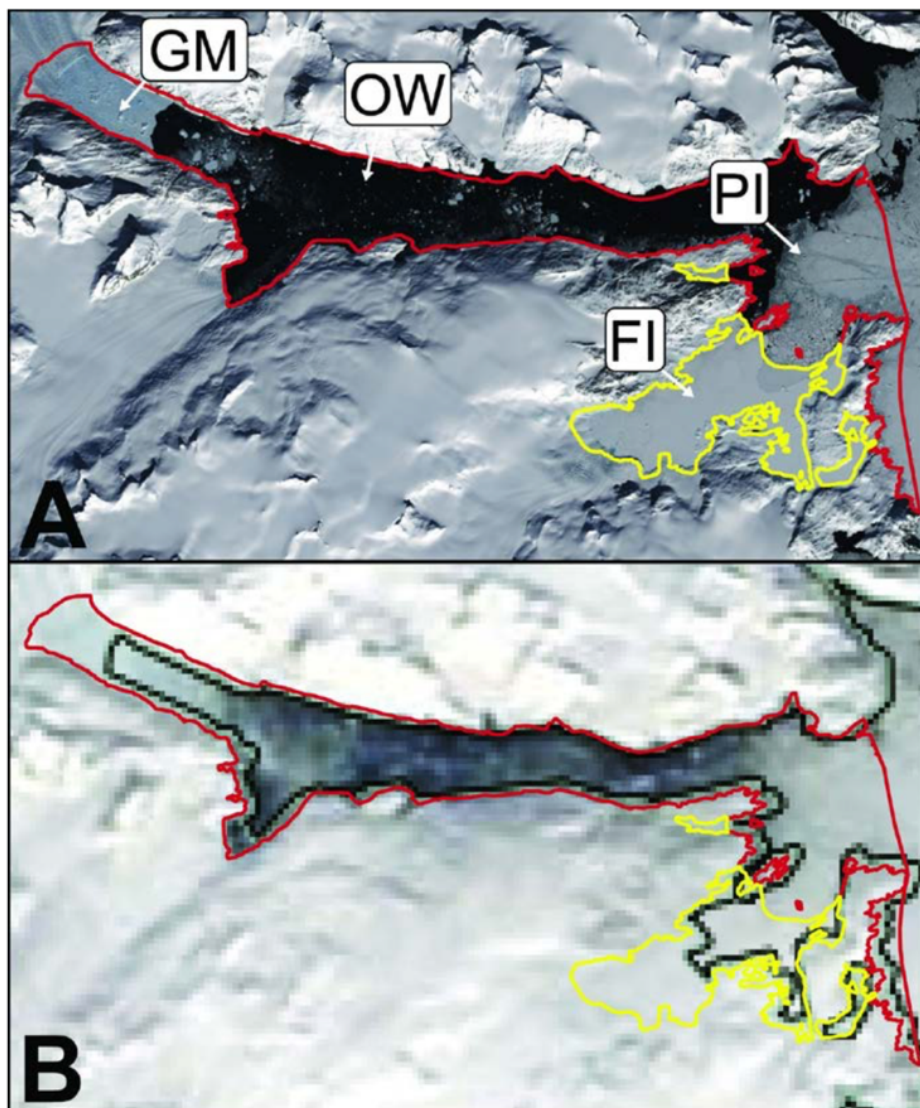


**Figure 4.** Example fast ice digitization. (a) Landsat 8 and (b) MODIS image examples for Anoritoq Fjord, both from 7 April 2017. Yellow outlines identify the fast ice areas and red lines indicate the rest of the fjord boundary. Note the distinct visual character of glacial mélange (GM), open water (OW), fast ice (FI), and pack ice (PI) (indicated in a). The misplacement of the coastline in the standard MODIS product is also apparent (b), and we use our own fjord boundary product for analysis. Figure reproduced from Laidre et al. (2022).

202 such images were available. The MODIS imagery was processed afterwards, using the results of the Landsat 8 analysis as a  
203 guide for the characterization of MODIS imagery. This facilitated increased accuracy of digitization within areas of  
204 ambiguous interpretation (as described below).



205 To quantify the degree of error introduced by using MODIS when Landsat 8 was unavailable, we digitized 25 MODIS  
206 images (analyzing 1 image from 2015-2019 for Skjoldungen, Timmiarmiut, Naparsuaq, Anoritoq, and Kangerluluk fjords)  
207 captured on the same date as Landsat 8 images already analyzed. We found a mean difference between the results of MODIS  
208 and Landsat 8 digitization of 1.2 km<sup>2</sup> of fast-ice area and a standard deviation of 12.6 km<sup>2</sup>. These levels of disagreement  
209 have no significant impact on our conclusions.

210 Based on early results, landfast sea ice boundaries were analyzed starting on January 1 until either July 1 or ice-free  
211 conditions were reached (whichever was first) from 2015 through 2019. We manually delineated landfast-ice boundaries for  
212 each available image. Based on visual analysis, we traced landfast-ice boundaries (without regard to fjord edge boundary)  
213 and recorded the date and source of the image. Any portions of the resulting polygons outside of the fjord boundaries were  
214 erased using the Clip (Analysis) tool in ArcGIS, which resulted in fjord-surface measurements of landfast-ice area and  
215 percent area coverage. This method precluded repetitive and time-consuming fjord boundary tracing, allowing for rapid  
216 digitization of landfast ice.

217 After calculating the landfast-ice area in a fjord system from all available imagery within a single year, we applied a moving  
218 average to obtain a smooth representation of the formation and breakup of landfast ice. The moving average on day  $t$  is  
219 calculated using weights proportional to  $\exp(-\Delta t^2/T^2)$  where  $\Delta t$  is the number of days from  $t$  to other data points, and  $T$  is a  
220 time scale equal to 7 days. To demonstrate the likelihood of landfast ice presence in any given spatial region across all  
221 observations, we also produced “heatmaps” of landfast sea ice presence (Figs. 10-13a,c) by overlaying all individual spatial  
222 occurrence maps and applying a gradient of shading (applying grid cell size of 50 m x 50 m).

### 223 **3.5 Glacier-derived ice for 8 focus fjords**

224 To analyze glacier-derived ice, we again used USGS Landsat 8 data imagery (following section 3.4 methods). The low  
225 spatial resolution of MODIS imagery made it unsuitable for this analysis. Because glacial ice has a year-round presence, we  
226 analyzed glacial ice presence from 1 January 2015 to 31 December 2019 for each year (Fig. 3b).

227 We characterized glacier-derived ice using four primary categories (Fig. 5, Table 2): spatially dense glacial ice mélange  
228 (type 3); moderately high-spatial-density, mixed-size glacier-derived ice with large icebergs (type 2); low-spatial-density  
229 glacier-derived ice with large icebergs (type 1); and consistent small-ice surface without large icebergs (type 0). (We also  
230 used a ‘type 99’ classification for glacier ice not yet calved). To measure the temporal and spatial distribution of glacier-  
231 derived ice in SEG, we analyzed the optical satellite imagery from Landsat 8 using the same ArcGIS 10.8 method as  
232 described for landfast sea ice for each glacier-derived ice type (Table 2). For the heatmaps of glacial ice presence (Figs. 10-  
233 13b,d), we combine spatial extent for type 2 and type 3 glacier-derived ice. This is motivated by an assessment that type 2  
234 and type 3 glacier-derived surface ice is more feasible for use as polar bear habitat platforms (e.g., Laidre et al., 2022).

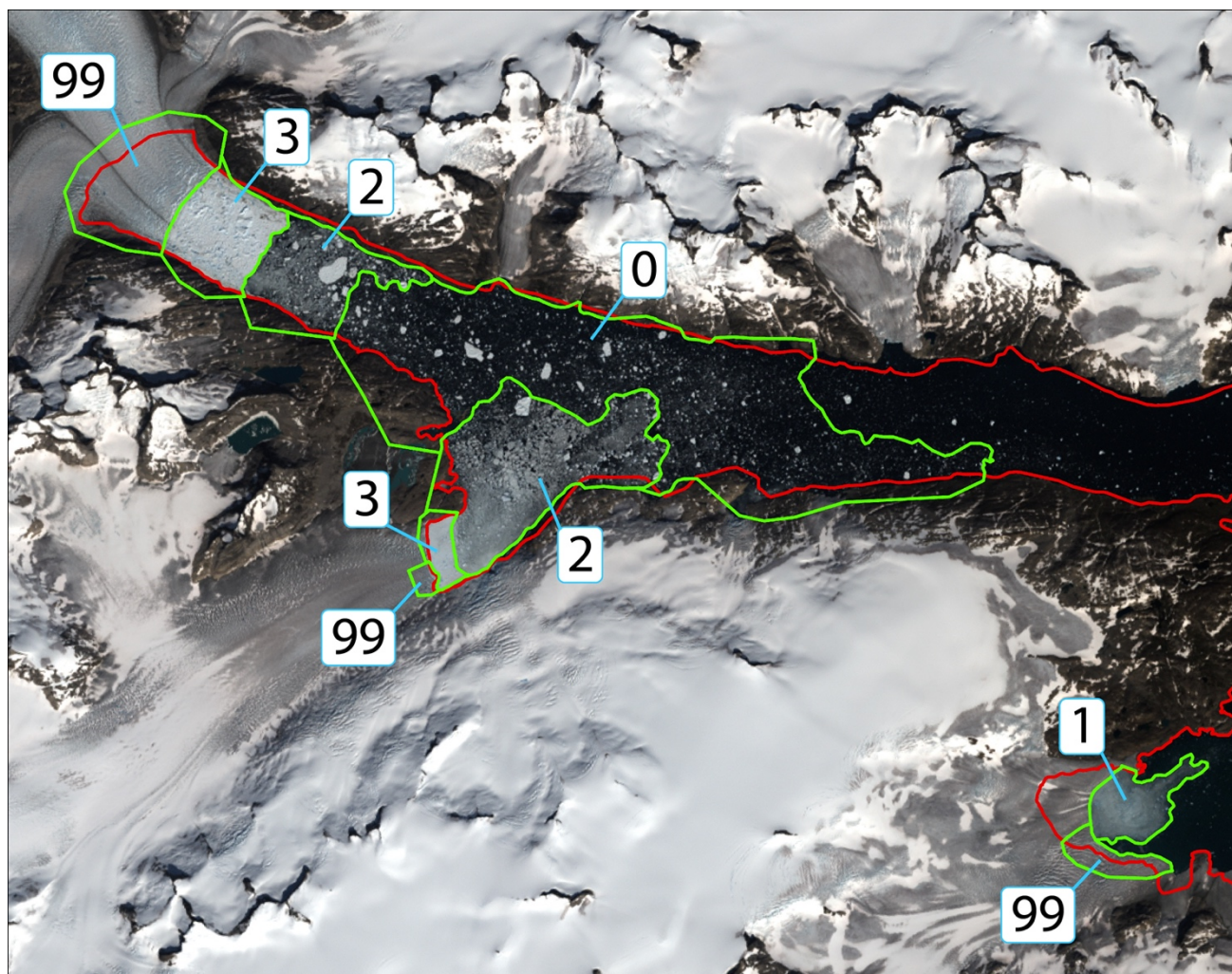


Figure 5. Example glacial ice digitization for Anoritoq fjord (fjord #45). Landsat 8 (8/1/15) background image showing the fjord boundary (red outline) and the digitized zones of different glacier-derived ice types on the fjord surface (green outlines and type indicated): type 3 (dense glacial mélange), type 2 (mixed glacier-derived ice), type 1 (small glacier-derived ice), type 0 (highly dispersed glacier-derived ice), and type 99 (glacier surface) (see Table 2). The boundaries are combined to determine final values for glacier-derived ice area.

#### 235 4 Results

236 This study includes data sets that span Southeast Greenland and metrics assessed only for the eight focus fjords. This supports  
237 some SEG region-wide analysis and further analysis to include more ocean-surface ice metrics for the eight focus fjords. Along  
238 with providing a more complete picture of the SEG environment, these results can support ongoing research into the current  
239 and future biological uses of SEG coastal fjords.



**Table 2: Glacier-derived fjord ice types as applied in this analysis.**

Glacial Ice Type	Description Used for Manual Digitizing
Type 3 (dense glacial mélange)	White to pale to blue color. Color (considering variation in texture) consistent throughout with bright, vibrant character Appears potentially cohesive, without open water gaps. May have sharp edge boundaries Texture: clear inclusions of many icebergs Also digitize very large (~>1km width) mélange platforms
Type 2 (mixed glacier-derived ice)	Majority of ice colored grayish blue of varying shades with semi-transparent character Discernible floes of apparently glacial origin, varying size with inconsistent cohesion and potential presence of small (~<250 m) open water gaps. Possible presence of Type 3 platforms Includes sizable icebergs
Type 1 (small glacier-derived ice)	Gray blue to dark blue coloration with higher degree of transparency compared to Type 2 and Type 3 ice Little to no cohesion, but still high spatial concentration of likely growlers/bergy bits. Few icebergs and Type 3 platforms of any substantial size, but not absent
Type 0 (highly dispersed glacier-derived ice)	Concentration of icebergs of moderate size (~250 m width) > 10% and <30% Little slushy (grey) background ice (bergy bits, growlers)
Type 99 (glacier surface)	Glacier surface. Sections of glacier ice not yet calved but inside the fjord boundary.

#### 240 4.1 Regional-scale observations

241 Datasets for offshore sea ice, freshwater flux, and solid ice discharge support an examination of conditions across the full SEG  
 242 region of interest.

##### 243 4.1.1 Offshore sea ice

244 Figure 6 shows the spring and fall transition dates for offshore sea ice at each fjord. First, while there is substantial year-to-  
 245 year variability in the spring transition dates, which range from May to early August, there is little variability with latitude  
 246 for a given year. In other words, offshore sea ice tends to disappear from the coast of SE Greenland in spring over a  
 247 relatively short time interval across all latitudes, but the timing of that disappearance varies from year to year. Second, the  
 248 arrival of offshore sea ice in the fall has a narrower range of interannual variability, but there is a distinct dependence on  
 249 latitude, with sea ice arriving in October at the more northerly fjords and in January or early February at the more southerly  
 250 fjords. The different nature of the spring and fall transition dates may be due to the relative influence of thermodynamics vs.  
 251 dynamics. In spring, rising temperatures along the coast may melt the sea ice at more-or-less the same time at all latitudes.  
 252 But in fall, the arrival of sea ice is due to transport from the north (via the East Greenland Coastal Current) rather than  
 253 freezing in place. A sea-ice “front” progresses from north to south every fall, at a speed of roughly 10 km day<sup>-1</sup> (Fig. 6). Note  
 254 that previous research identified that sea ice along the SEG coast had a mean wintertime (January-April) south-moving speed

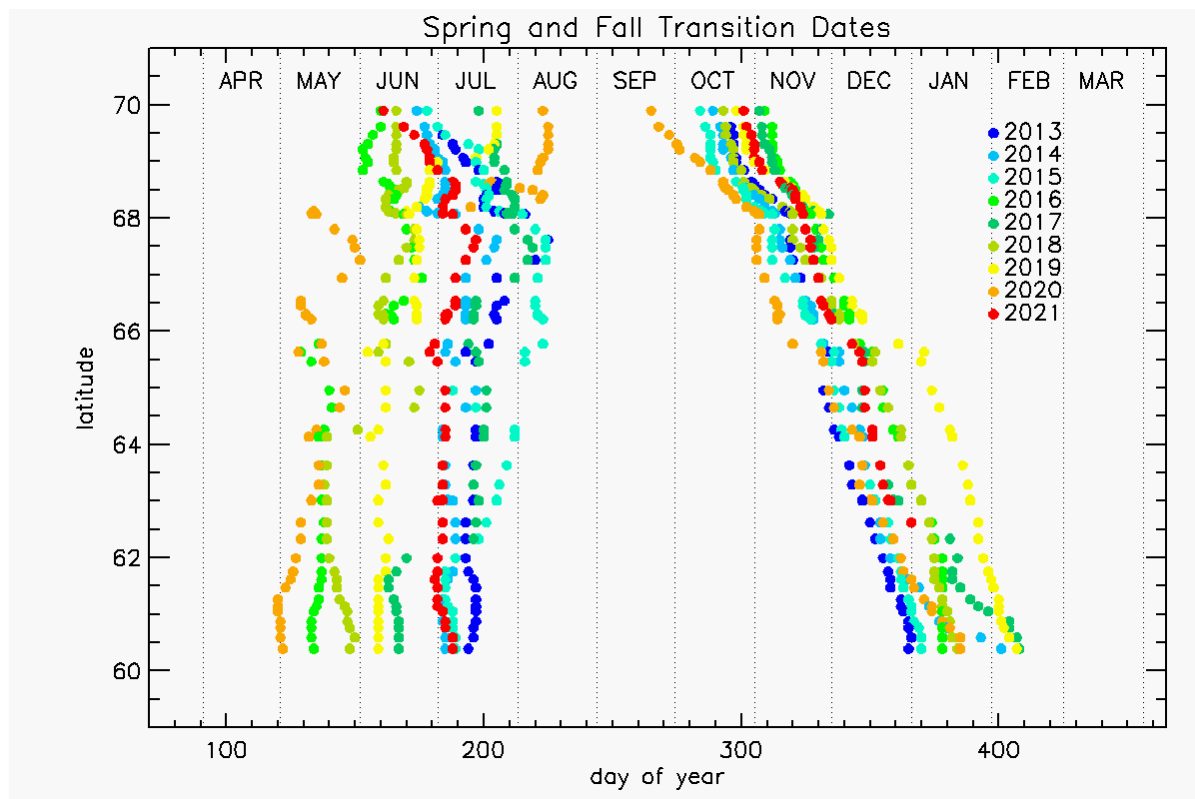


**Figure 6. Spring and fall transition dates of offshore sea ice for all fjords (by latitude) and years (by color) based on a 15% coverage threshold.**

255 of about  $15 \text{ cm s}^{-1}$  ( $13 \text{ km day}^{-1}$ ) from 2010 to 2018 (Laidre et al., 2022). In spring, the sea ice does not retreat along a well-  
256 defined front. Though the seasonal coverage and concentration of offshore sea ice during our study period is reduced from  
257 earlier decades (Heide-Jørgensen et al. 2022) and is expected to continue to shorten and decline, respectively (Kim et al.,  
258 2023), we suggest that the differences in spring and fall transitions may largely persist (while sea ice is still forming).

#### 259 4.1.2 Freshwater flux

260 Figure 7 shows freshwater flux on the fjord scale across SEG. The results show that there is large variability, from low total  
261 annual discharge of  $\sim 1 \times 10^8 \text{ m}^3$  ( $\sim 0.1 \text{ Gt}$ ) at fjords 6 and 44 up to  $\sim 1.25 \times 10^{10} \text{ m}^3$  ( $\sim 12.5 \text{ Gt}$ ) at Sermilik Fjord (fjord 30),  
262 though notably the next largest fjord freshwater fluxes are only  $8.48 \times 10^9 \text{ m}^3$  (8.48 Gt; Kangerdlugssuaq, fjord 18) and  
263  $7.12 \times 10^9 \text{ m}^3$  (7.12 Gt; Jens Munk, fjord 33). In the northern region of SEG, the catchment geography feeds much of the  
264 freshwater to fjord 5, while other fjords in that zone see little freshwater flux until reaching south to fjord 15 and then to  
265 fjord 18 (Kangerdlugssuaq). There's low to moderate flux for most fjords between 18 and 30 (Sermilik), with a notable  
266 increase in mean annual freshwater flux for a number of fjords south of Sermilik.

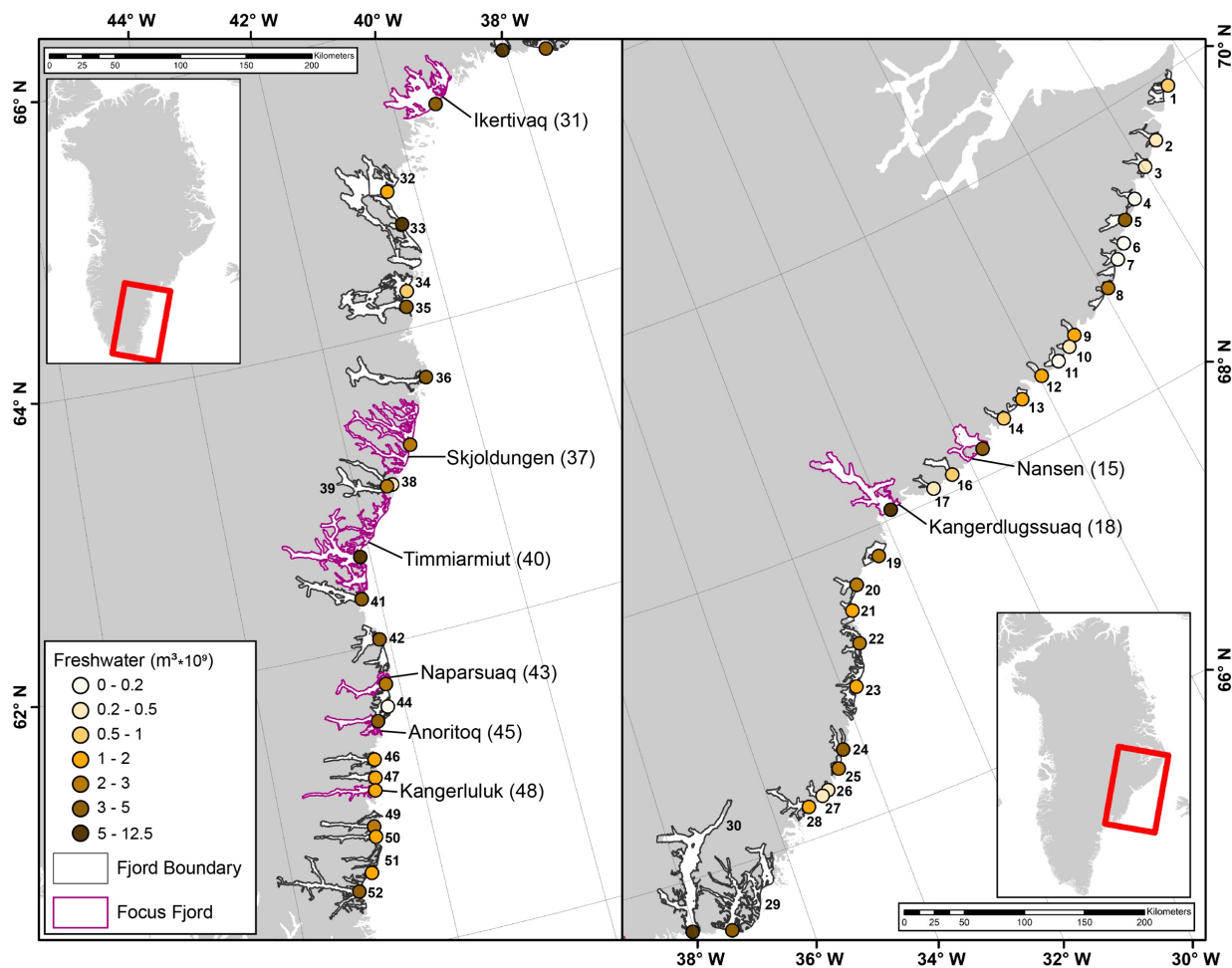


**Figure 7.** Mean total annual freshwater flux ( $\text{m}^3 \times 10^9$ ) for 2015 through 2019. The freshwater discharge is summed for the full fjord, including melt that originated from ice-covered and terrestrial areas and sourced from Mankoff (2020) and Mankoff et al. (2020a). Note that for freshwater,  $1 \text{ m}^3 \times 10^9$  volume is equivalent to 1 Gt weight.

267 Using the discharge elevation/depth, we were also able to assess how much freshwater was entering fjords at the ocean  
 268 surface or at depth, discharging from under marine-terminating glaciers. Across the SEG study region, the ocean surface  
 269 input and 0-20 m depth bins receive the most input when considering flux through sea level to 1000 m depth (Fig. A1).  
 270 Across the region and looking deeper into the water column, flux totals are highest within the top 100 m. While flux is  
 271 measured as deep as 900 m (fjord 31, Ikertivaq), most flux occurs at depths shallower than 600m. Strong seasonal variability  
 272 in freshwater flux is also apparent (e.g., Fig. 9c). Detailed individual fjord plots are available via our research code (see Code  
 273 and data availability).



274 **4.1.3 Solid ice discharge**

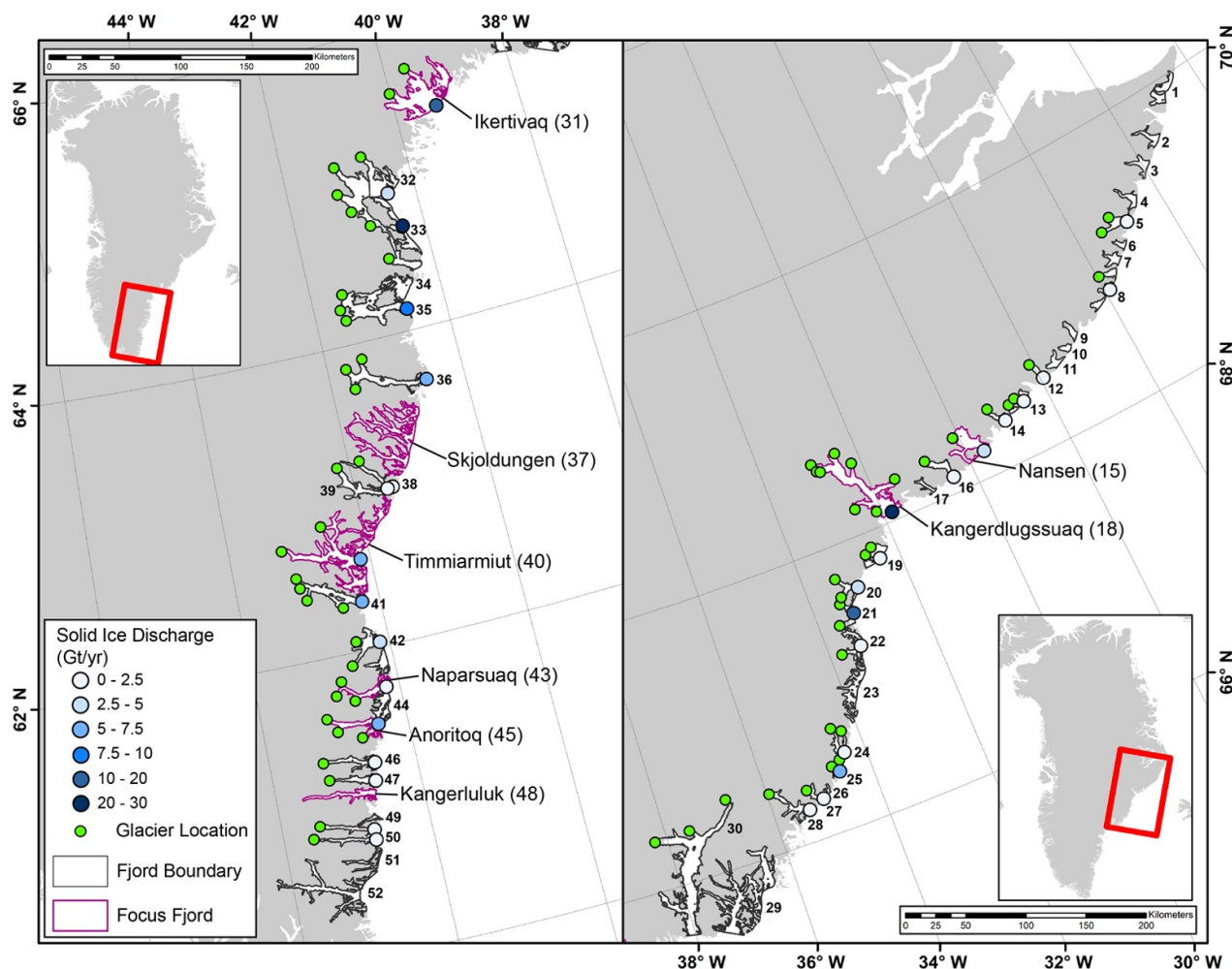


**Figure 8.** Mean annual solid ice discharge (Gt/yr) during 2015 through 2019 for glacier-derived ice from indicated glaciers, calculated using Mankoff et al. (2020b).

275 Figure 8 shows annual solid ice discharge estimates. We used a fjord-scale perspective to examine solid ice discharge and  
276 relied on the availability of glacier solid ice discharge data from Mankoff et al. (2020b, 2020c). Because of this, our solid ice  
277 discharge values may underestimate discharge or provide no data for a fjord in which some glacier-derived ice is variably  
278 present. For example, the source dataset contains no glacier discharge data for Skjoldungen fjord even though glacier-ice  
279 inputs are apparent in our satellite image analysis (Figs. A4 and 11d). Within the fjord dataset we were able to create (Fig.  
280 8), fjords north of Sermilik have relatively small annual contributions of glacier-derived ice, with the exception of  
281 Kangerdlugssuaq (fjord 18) and, to a lesser extent, fjord 21. Slow flow rates and often relatively thin glacier termini in this  
282 region are the cause of the low glacier-derived concentrations in many fjords, especially for the Geike Plateau, where most

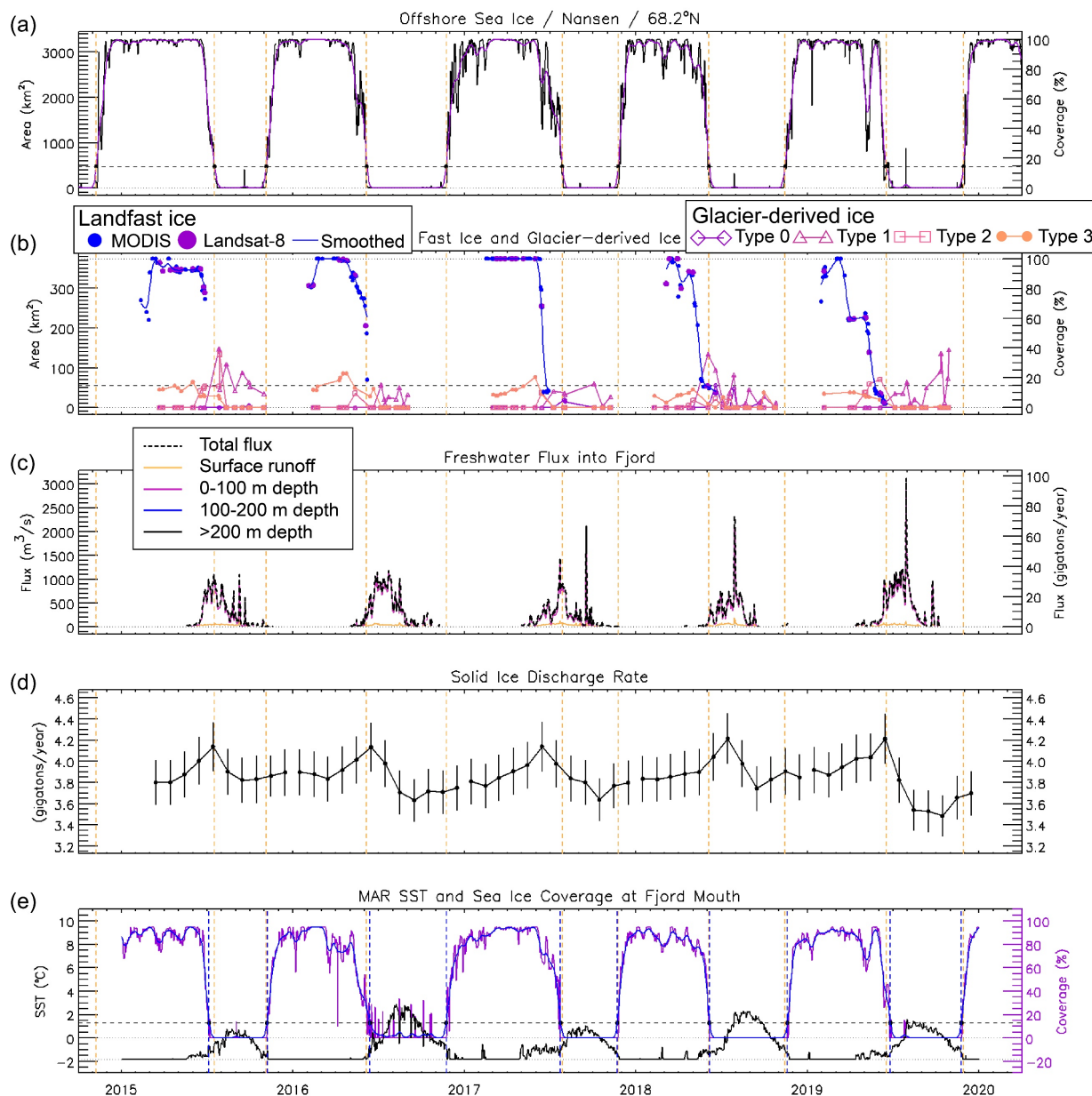


**Figure 9: Time series for fjord 15 (Nansen) showing: a) daily (black line) sea-ice area (km<sup>2</sup>) and percent coverage based on AMSR-2 sea ice concentration, along with a 31-day running mean (purple), b) area (km<sup>2</sup>) and percent coverage for landfast ice evaluated from MODIS (blue dot) and Landsat (purple dot) single image sources and with smoothed (blue) record and for all four surface character types (0-3) for glacier-derived ice, c) total freshwater flux (m<sup>3</sup> s<sup>-1</sup>, black dashed line) and depth-binned (solid line) freshwater flux, d) cumulative fjord solid ice discharge (Gt yr<sup>-1</sup>), and e) sea surface temperature (black line) and sea ice coverage (purple line) measured at the fjord mouth from MAR climate data. Vertical dashed orange lines in all panels indicate the freeze-up and break-up dates for offshore sea ice (panel a) as measured by passing a threshold of 15% of mean March-April sea ice area. A similar threshold is indicated (dashed line) in panel e, while panel b is a simple 15% threshold (dashed line). Similar figures are provided in Appendix A for other focus fjords.**

283 glaciers may be considered part of a peripheral ice cap (Rastner et al., 2012). By contrast, Ikertivaq and a number of fjords



284 south of Sermilik are fed by several glaciers, many of which receive moderate and greater levels of solid ice discharge.

#### 285 4.2 Focus fjord observations

286 Manual analysis of landfast sea ice and glacier-derived ice allows us to integrate these observations and compare across  
287 metrics. Figs. 9 and A2-8 provided stacked 2015-2019 time series of offshore sea ice area and percent coverage; landfast ice  
288 and glacier-derived ice area and percent coverage; freshwater flux binned into sea surface input and input at depths of 0-100  
289 m, 100-200 m, and >200 m; cumulative fjord solid ice discharge; and fjord mouth SST and sea ice coverage from  
290 MARv3.12. These give a sense of temporal evolution across a range of latitudes. In contrast, Figs. 10-13 hone in on results

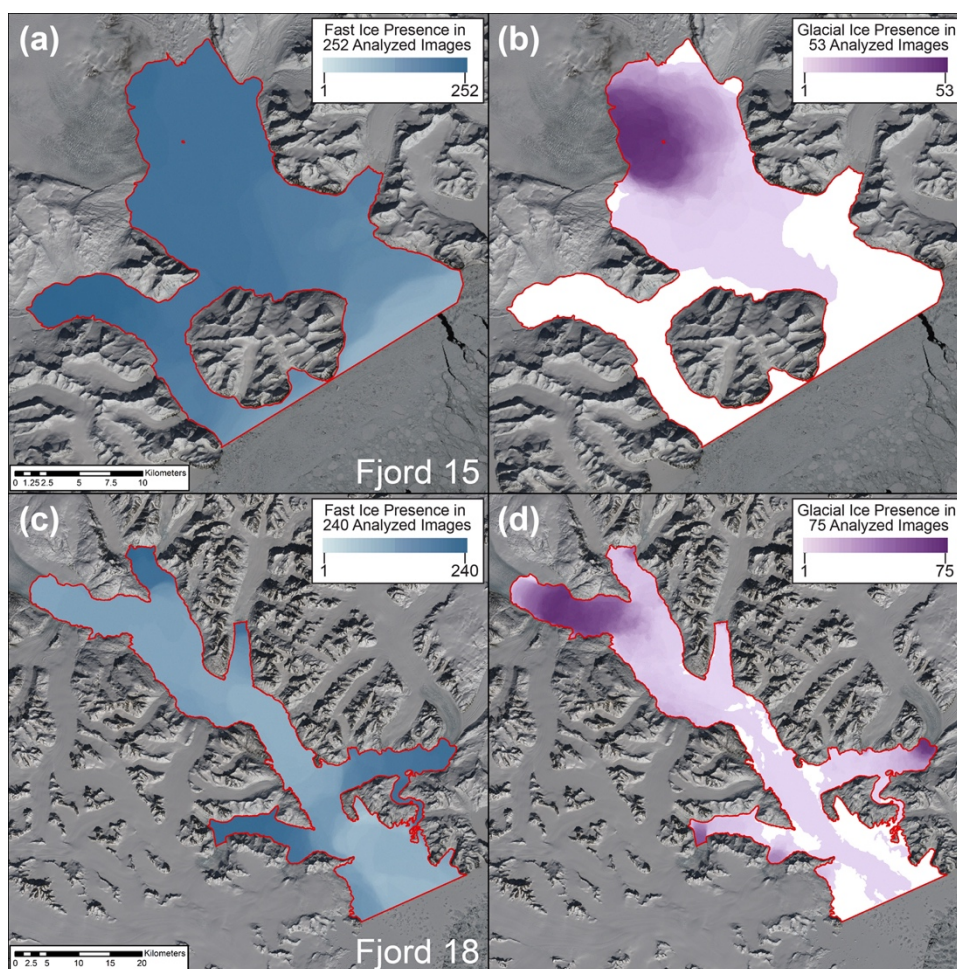


Figure 10. Maps of fast ice presence (a and c) and glacial ice presence for types 2 and 3 (b and d) for fjord 15 (Nansen, top panels) and fjord 18 (Kangerdlugssuaq, bottom panels). Map symbology is relative to the number of images analyzed (noted in panel legends).



291 of the landfast and glacier-derived ice analysis to provide a spatial map-view for the presence of landfast ice and types 2 and  
292 3 glacier-derived ice.

293 Across all eight focus fjords, landfast ice regularly accumulates in particularly narrow fjord "corridors" (narrow areas of the  
294 fjord with entrances/exits for ice flux on either end; e.g., Fig. 11a, c) and/or the "corners" of fjords (areas with a single  
295 entrance/exit for ice flux and a confined coastal topography; e.g., Fig. 12a, c). The Nansen (fjord 15) and Kangerdlugssuaq  
296 (fjord 18) fjords display periods in which they are fully covered by landfast ice in certain years, while all the more southerly  
297 fjords do not reach full landfast ice coverage in any study years.

298 Despite broad seasonality and spatial consistency to landfast ice development, there is substantial year-to-year variability for  
299 landfast ice development within each fjord (panel b within Figs. 9 and A2-8). When considering a 15% landfast ice coverage

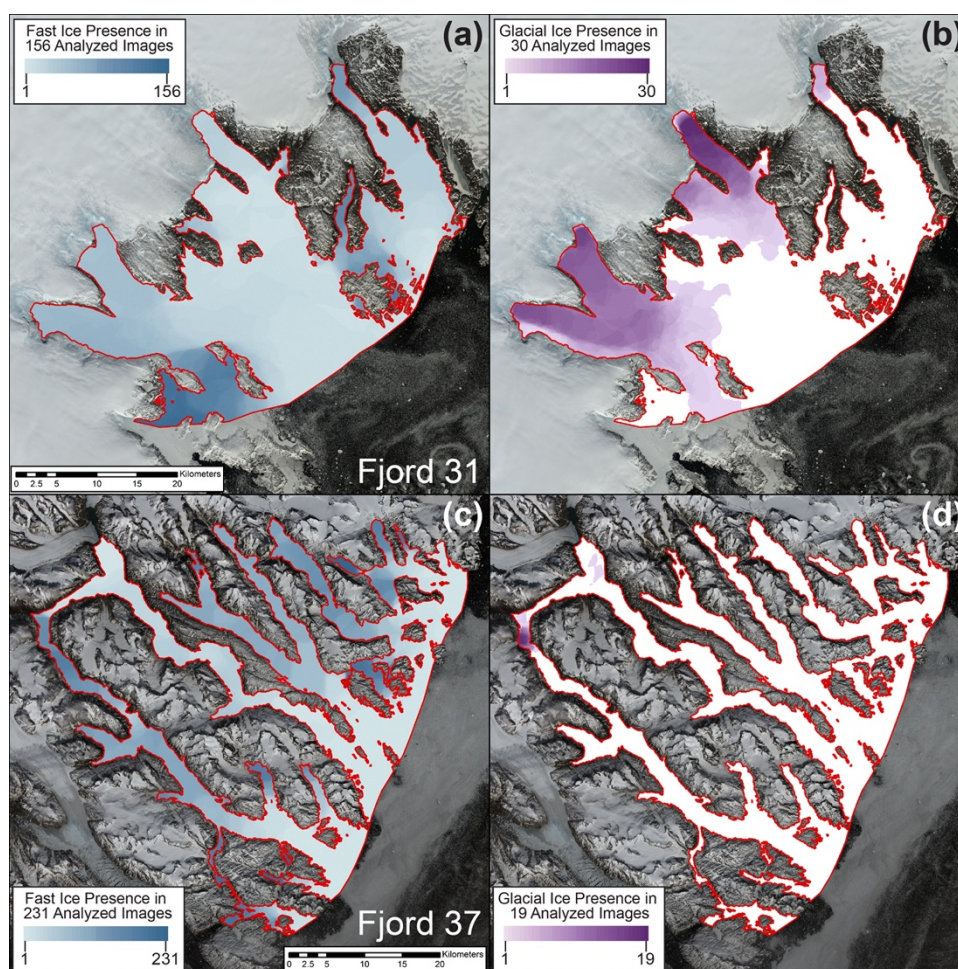


Figure 11. Same as figure 10 for fjord 31 (Ikertivaq, top panels) and fjord 37 (Skjoldungen, bottom panels).



300 threshold, more northern five focus fjords have lower variability in the timing of landfast ice development and breakup, but  
301 the timing of the fast-ice peaks have substantial variability (Table A1). For example, in 2017 in Ikertivaq the landfast ice was  
302 slower to form, with some expansion/decline, before peaking at close to 80% area coverage in late April, while in 2019  
303 Ikertivaq experienced a relatively rapid development of landfast ice with a similar area coverage peak in early March (Fig.  
304 A3). For the three southernmost fjords there is larger variability in the timing of the formation and breakup of the landfast  
305 ice. Landfast ice did not surpass a 15% ice coverage threshold for Naparsuaq in 2019, Anoritoq in 2015, and Kangerluluk in  
306 both 2015 and 2019 (Figs. A6-8). Yet, we do observe clear instances of landfast ice remaining in place well-after offshore  
307 sea ice has fully disappeared, with many of the focus fjord declines in landfast sea ice lagging the offshore sea-ice declines  
308 by more than a month in 2016 and ~two weeks in 2018 (panel b within Figs. 9, A2-8).

309 Glacier-derived ice presence for types 2 and 3 combined (Figs. 10-13b,d) is dependent on marine-terminating glacier  
310 locations, with higher presence near the glacier termini. As expected, the manually digitized imagery also highlights glacier

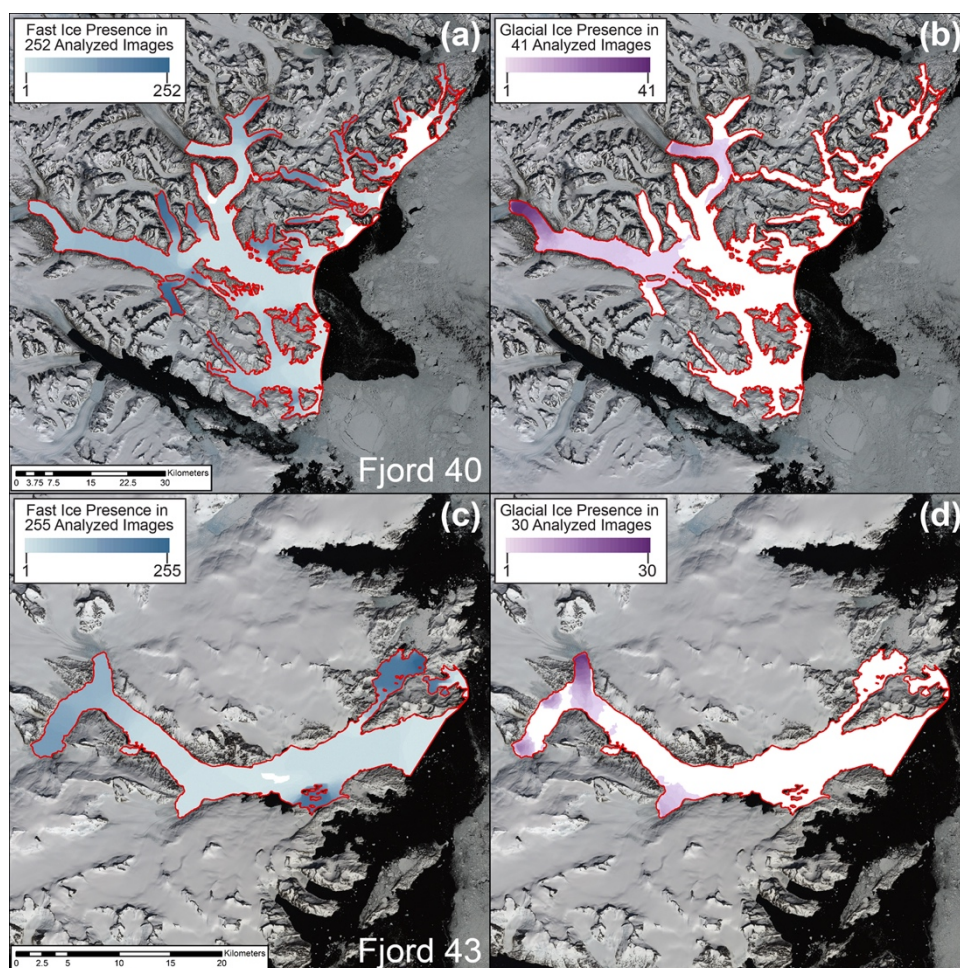


Figure 12. Same as figure 10 for fjord 40 (Timmiarmiut, top panels) and fjord 43 (Naparsuaq, bottom panels).



311 ice inputs that may be absent in other datasets (such as we use for regional SEG solid ice discharge). Because of landfast ice  
312 and glacier-derived ice intermixing (or at minimum an inability to distinguish boundaries from satellite imagery), our results  
313 highlight glacier-derived ice-dominant or landfast ice-dominant fjord regions rather than consistent or clear delineations  
314 within most fjord regions. The time series of glacier-derived ice (Figs. 9, A2-8) indicate that only Kangerdlugssuaq,  
315 Ikertivaq, and Anoritoq more regularly contain types 2 and 3 glacier-derived ice outside of that fjord's landfast ice season.

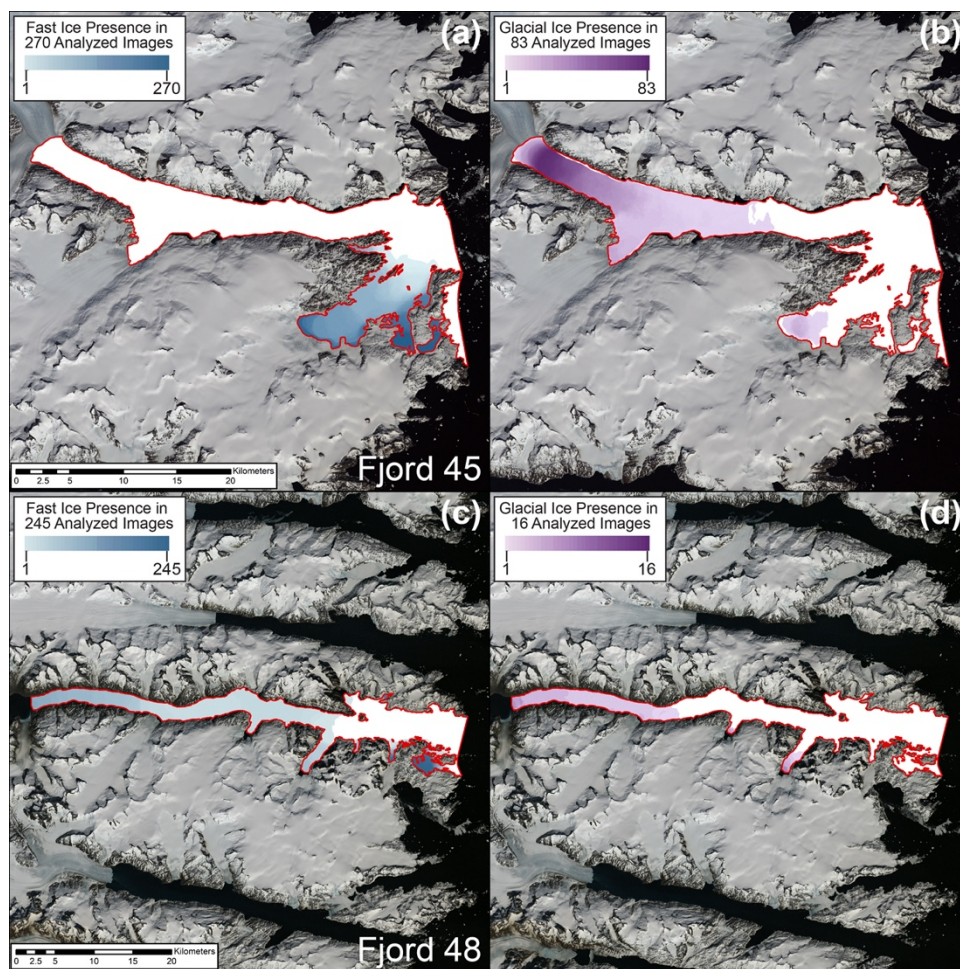


Figure 13. Same as figure 10 for fjord 45 (Anortioq, top panels) and fjord 48 (Kangerluluk, bottom panels).

#### 316 4 Discussion

317 Factors affecting ice in SEG fjords can be broadly divided into two categories: (1) fixed factors such as fjord width, length,  
318 bathymetry, orientation, latitude, and locations of glaciers feeding into the fjord; and (2) variable factors such as katabatic  
319 winds coming off the ice sheet, along-shore winds driven by cyclones, ocean currents, ocean stratification, ocean heat



320 content, air temperature, formation of sea ice, and the discharge of freshwater and glacial ice into the fjord. The formation of  
321 landfast ice and accumulation of glacier-derived ice in SEG fjords tends to have a semi-consistent spatial pattern; landfast ice  
322 and glacial ice can be found in similar areas within each individual fjord from year to year (Figs. 10-13). This distribution is  
323 likely a combination of fixed and variable factors. For example, the morphology of each fjord system is likely a first order  
324 control. Variable factors such as ocean currents may also produce relatively consistent ice conditions, but current and future  
325 potential for ocean variations have to be considered. For example, as the East Greenland Coastal Current flows past the  
326 mouth of a fjord, it turns to the right (due to Coriolis) and enters the fjord, keeping the shoreline on the right. The current  
327 flows into the fjord along the north or east side of the fjord, then out along the south or west side of the fjord, influencing  
328 ice-forming surface conditions and iceberg motion in the process. But the flow is not steady in time. Recent examination of  
329 four East Greenland fjords, including two in SEG (Kangerdlugssuaq and Sermilik), found periodicity in current patterns in  
330 the range of 2-4 days for Kangerdlugssuaq, plus a broad peak around 10 days (Gelderloos et al., 2022). Thus, factors still not  
331 included in this study warrant examination and future synthesis.

332 Temporally, landfast ice and glacial ice follow different patterns. Landfast ice forms seasonally from roughly February to  
333 late May, with significant inter-annual variability of cover duration (Table A1), while glacier-derived ice can be found in  
334 various fjords year-round (Laidre et al., 2022). However, the character (e.g., type 0-3), timing, and area coverage of glacier-  
335 derived ice is strongly fjord-dependent, with even some glacier-fed fjords appearing to provide little possibility for  
336 substantial glacier-derived ice habitat outside of the landfast ice season.

337 Of note regarding our mapping of landfast ice locations is that they commonly appear in areas that remain poorly mapped for  
338 bathymetry. Comparing landfast ice locations with bathymetric data from BedMachine 5 (Morlighem et al., 2017;  
339 Morlighem et al., 2022), for example, landfast ice often occurs in presumably shallow regions that lack any bathymetric  
340 detail. Greenland sea level responses to climate change include the possibility for local regions to experience falling sea  
341 levels (Fox-Kemper et al., 2021). This suggests that understanding shallow-region bathymetry will only become more  
342 important, though the sea level changes may occur much slower than some other global coasts. For example, changes in  
343 ocean depth have the potential to influence wave character, which contributes to mechanical landfast ice breakup (Petrich et  
344 al. 2012), and the prevalence of possible grounding points, which may influence landfast ice formation (Mahoney et al.  
345 2014).

346 Glacier-derived ice, produced from marine-terminating glaciers in SEG fjords, is initially deposited at the glacier terminus  
347 and proceeds to drift into the fjord as it melts, fractures, and disperses. As glacial ice travels through the fjord system, it can  
348 become trapped amongst forming landfast ice and thus effectively adding to the landfast ice itself. This is especially frequent  
349 in narrow, long fjords where landfast ice can clog passageways and prevent glacial ice from exiting the fjord at the mouth.  
350 This heterogeneous mixture of frozen fast ice and glacial ice provides stable optimal springtime habitat for ice-breeding  
351 seals, as well as foraging polar bears (Laidre et al., 2022). The distribution of glaciers across SEG (e.g., Fig. 1) is  
352 heterogeneous, with some fjord systems having multiple productive glaciers (e.g., fjords 18 and 31) while others have minor



353 or no glacier-derived flux (e.g., fjord 37). It is unclear from our observations the extent to which glacier-derived ice either  
354 enhances landfast ice persistence or diminishes it. For example, production of glacial ice in fjord 15 may help to compress  
355 and possibly thicken landfast ice (Fig. 10a,b), especially if paired with sea ice circulating into the fjord from offshore. On the  
356 other hand, glacial ice traversing from a glacier terminus towards the fjord mouth might shear against the landfast ice edges,  
357 particularly if they are subject to different wind or current forces, for example due to different surface heights and bottom-ice  
358 depths.

359 Differences in offshore sea ice and landfast ice development across SEG suggest that glacier-derived ice may be especially  
360 important as a fjord surface ice environment. Earlier research demonstrated that the 1999-2018 mean width of the wintertime  
361 sea-ice band for 60-65°N was 19 km, while for 65-70°N it was 149 km (Laidre et al. 2022). The four most southerly focus  
362 fjords functionally experienced no full coverage of offshore sea ice throughout 2015-2019 (Figs. 9a, A2-8a). Combined with  
363 low landfast ice coverage, animals may have limited options for sea ice platforms, while glacier-derived ice is present to  
364 some extent in all of these fjords. The extent to which limited and sporadic coverage of glacier-derived ice (Figs. 9b and A2-  
365 8b) provides year-round ice habitat is unknown, but observations and tracking data of top predators suggests animals use this  
366 habitat year-round for hauling out (e.g., resting) or foraging (Laidre et al., 2022).

## 367 **5 Conclusion**

368 Fjords across Southeast Greenland exhibit high fjord-to-fjord variability in regards to bathymetry, size, shape, and glacial  
369 setting. As a result, some fjords receive substantially higher annual freshwater flux from ice sheet/glacier and terrestrial  
370 runoff, as well as fjords with much higher presence of glacier-derived ice. The inputs mix with in-fjord sea ice and landfast  
371 ice and offshore sea ice to create a dynamic fjord surface environment.

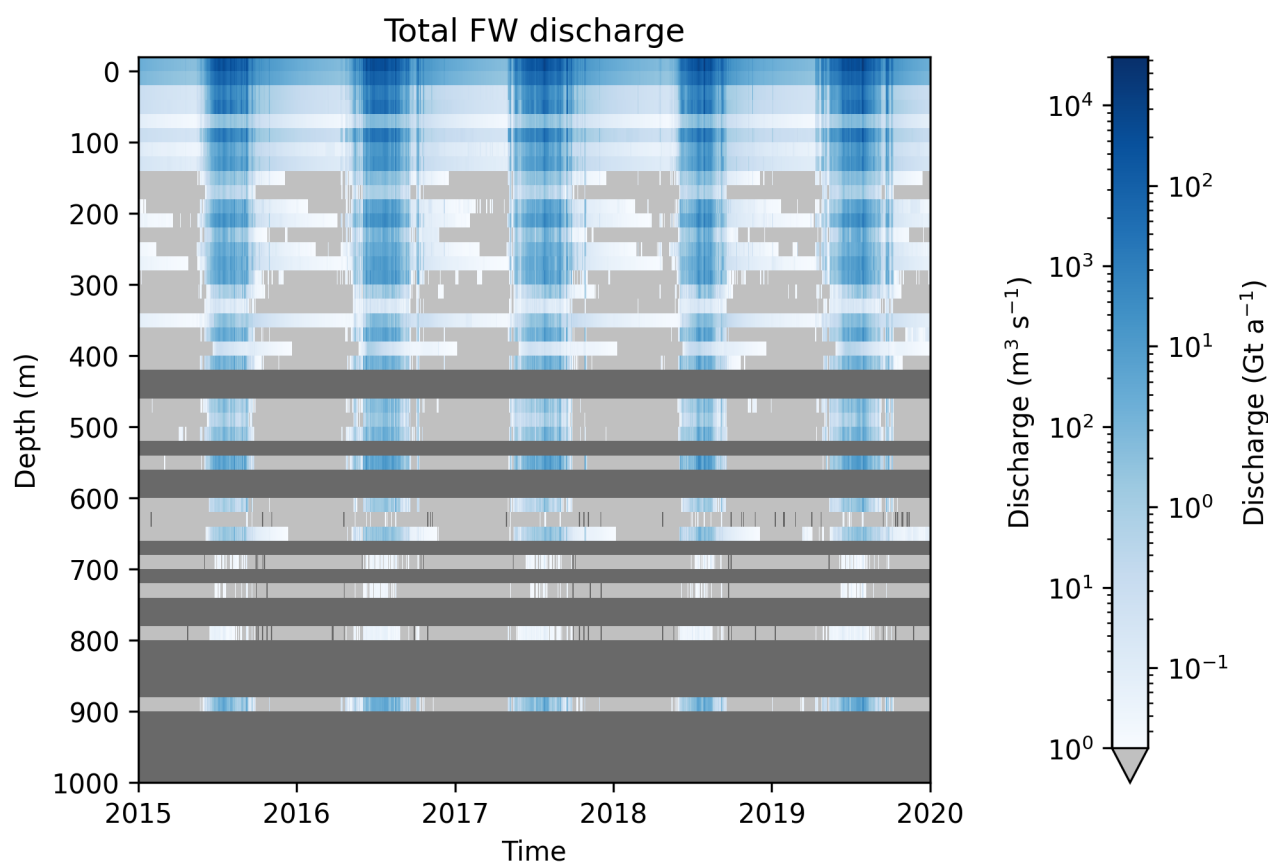
372 Across 2015 through 2019, SEG fjords demonstrate substantial year-to-year variability. While the impacts of climate change  
373 may be expected to push long-term trends in one general direction, the variability in separate metrics will likely be different.  
374 For example, the sensitivity of freshwater flux to ice sheet surface melt introduces a high dependency on atmospheric  
375 conditions, which change rapidly and have high inter-annual variability (Lenaerts et al., 2019). On the other hand, solid ice  
376 discharge depends on ice sheet and glacier dynamics, which generally respond more slowly to climate change and have  
377 lower inter-annual variability (Moon et al., 2022), and ocean conditions. Landfast sea ice variability introduces further  
378 dependence on ocean surface conditions, which are also a major factor for formation of mobile sea ice.

379 With sea ice loss well underway along the SE Greenland coast and projections for summer sea-ice free conditions to occur  
380 within one to two decades (Kim et al. 2023), the importance of glacier-derived ice as a habitat for top predators may only  
381 rise. Projections for the spatial patterns of Greenland Ice Sheet retreat under a range of future scenarios point towards the  
382 longer-term presence of glacier ice in SEG compared to other areas on the coast (Aschwanden et al., 2019; Bochow et al.,  
383 2023). High winter precipitation in SEG as compared to other regions (Gallagher et al., 2021) is one important factor in

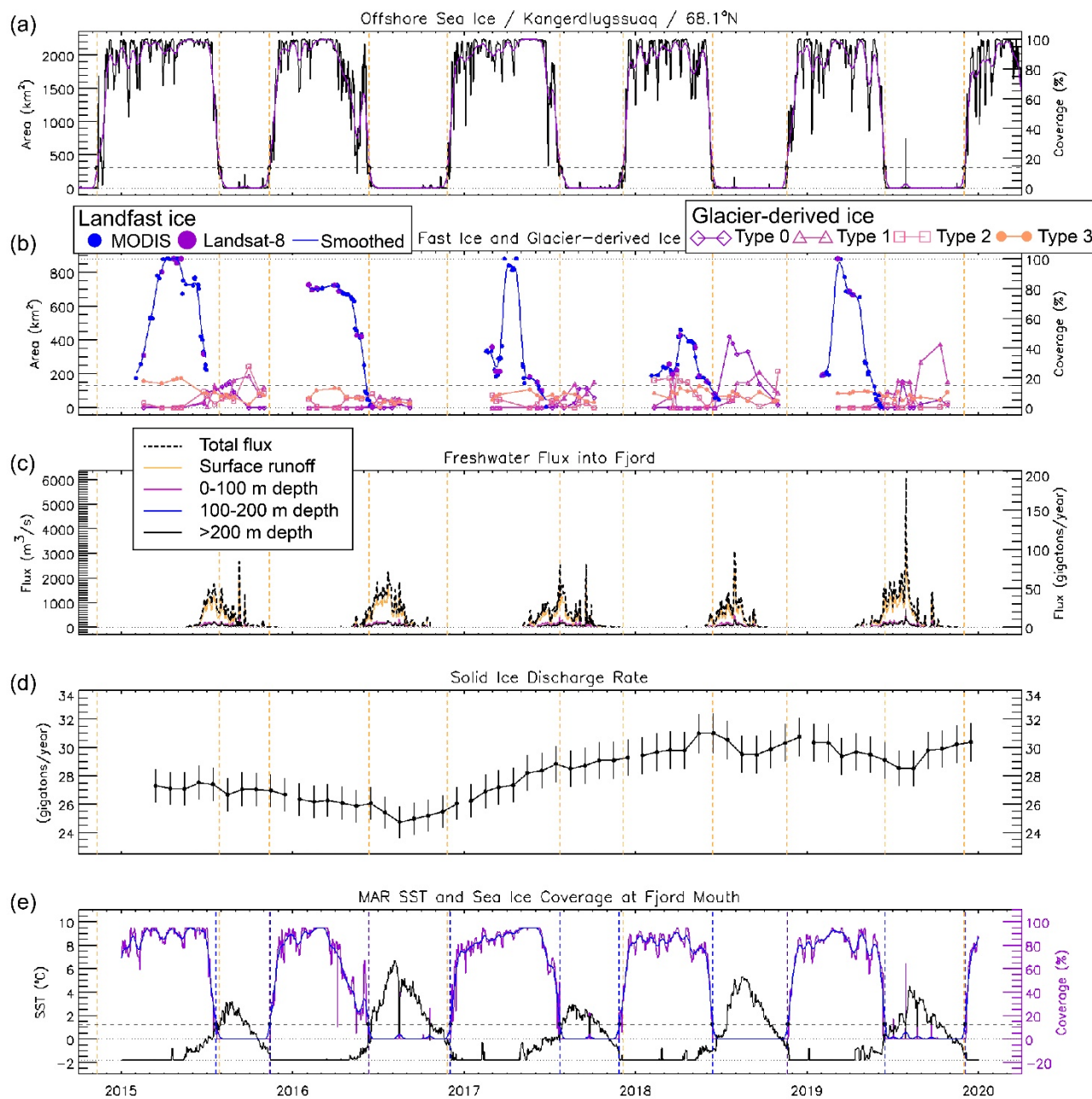


384 sustaining glacier ice in the region. This higher regional winter snowfall may also provide longer-term habitat appropriate for  
385 ringed seal birthing lairs, which are created as on-sea-ice snow caves with sufficient snow cover associated with lower  
386 predation rates (Kelly et al., 2010). Further, the heterogeneous mix of glacial ice frozen into the fast ice can provide suitable  
387 drifts for ice seal birth lairs, which can form quickly on any side of an iceberg given their complex geometry. This has also  
388 been seen in the case of polar bear maternity dens in Northeast Greenland (Laidre and Stirling 2020). As a result, there is a  
389 potential for SEG to remain a long-term (century to millenia scale, dependent on future climate change pathway) refugia  
390 location for polar bears and other ice-dependent wildlife, but further investigation is required to quantitatively assess this  
391 potential.

392 **Appendix A**



393  
394 **Figure A1.** Total freshwater (FW) discharge within SEG fjords during 2015 through 2019, representing only data within Mankoff  
395 (2020) and Mankoff et al. (2020a). Freshwater discharge is binned into 20-m segments, from +20 – 0 m asl (above sea level) to 980 –  
396 1000 m depth, with all discharge from elevations above 0 m asl included in the +20 – 0 m asl bin. Light gray areas indicate times  
397 when the discharge in that bin was below a discharge threshold of 1 m<sup>3</sup> s<sup>-1</sup>, while dark gray areas indicate no data were available.



398

399

400

401

402

403

404

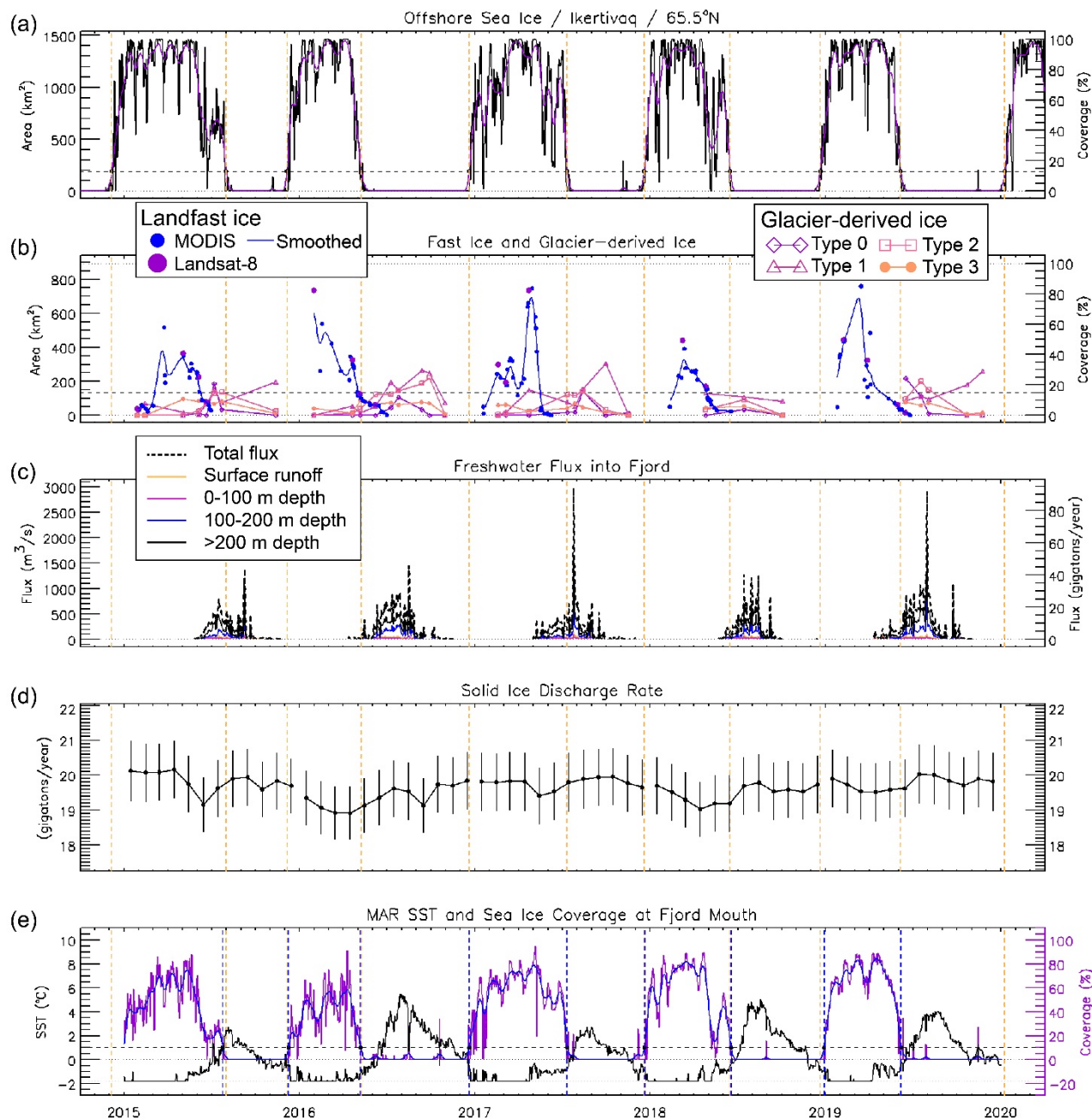
405

406

407

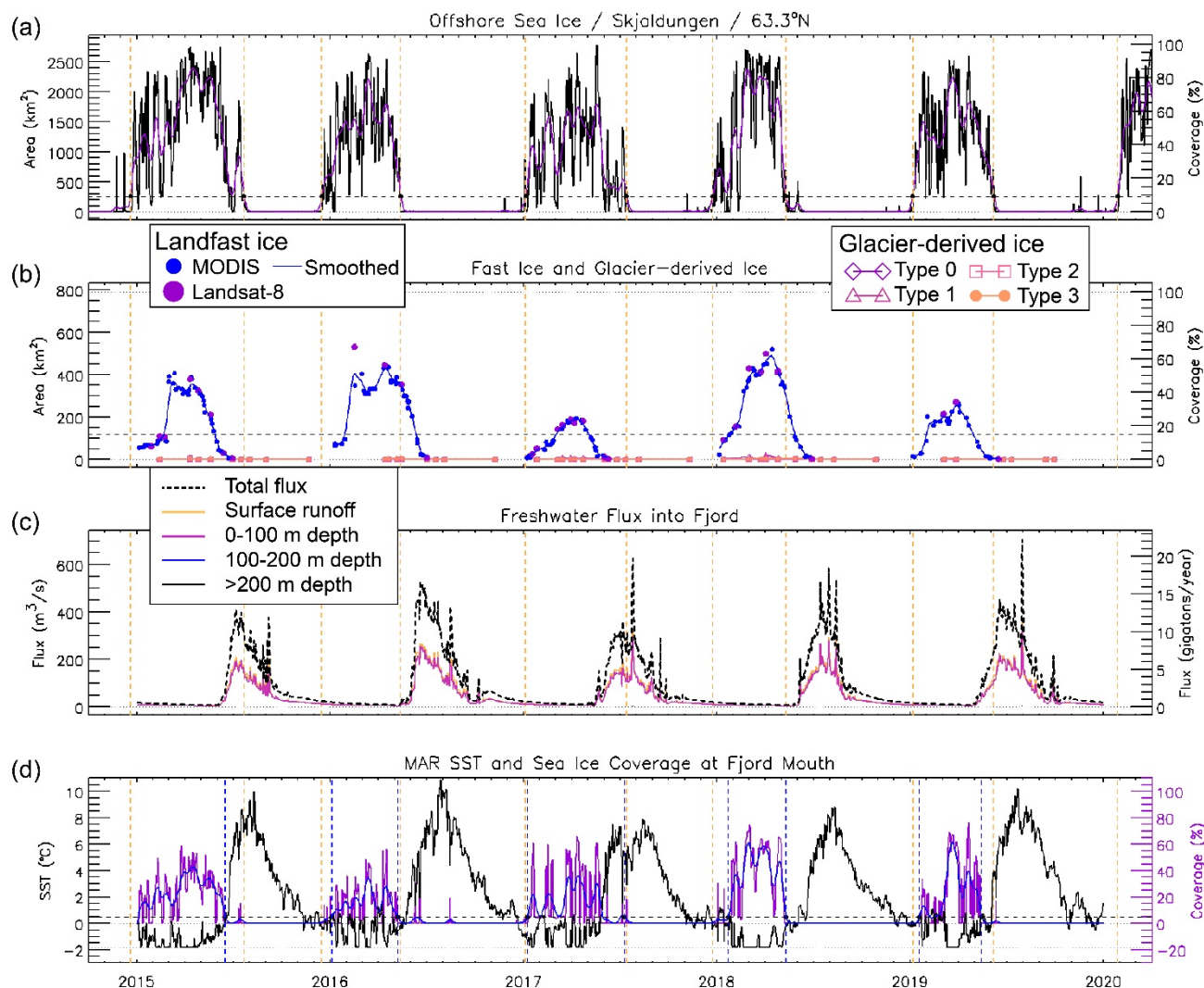
**Figure A2.** Time series for fjord 18 (Kangerdlussuaq) showing: a) daily (black line) sea-ice area (km<sup>2</sup>) and percent coverage based on AMSR-2 sea ice concentration, along with a 31-day running mean (purple), b) area (km<sup>2</sup>) and percent coverage for fast ice evaluated from MODIS (blue dot) and Landsat (purple dot) single image sources and with smoothed (blue) record and for all four surface character types (0-3) for glacier-derived ice, c) total freshwater flux (m<sup>3</sup> s<sup>-1</sup>, black dashed line) and depth-binned (solid line) freshwater flux, d) cumulative fjord solid ice discharge (Gt yr<sup>-1</sup>), and e) sea surface temperature (black line) and sea ice coverage (purple line) measured at the fjord mouth from MAR climate data. Vertical dashed orange lines in all panels indicate the freeze-up and break-up dates for offshore sea ice (panel a) as measured by passing a threshold of 15% of mean March-April sea ice area. A similar threshold is indicated (dashed line) in panel e, while panel b is a simple 15% threshold (dashed line). The 15% threshold is indicated by a dashed line in panels a, b, and e.

408



409  
410

Figure A3. Same as Fig. A2 for fjord 31 (Ikertivaq).



411  
 412

Figure A4. Same as Fig. A2 for fjord 37 (Skjoldungen), but with no solid ice discharge data and panel (e) presented as panel (d).

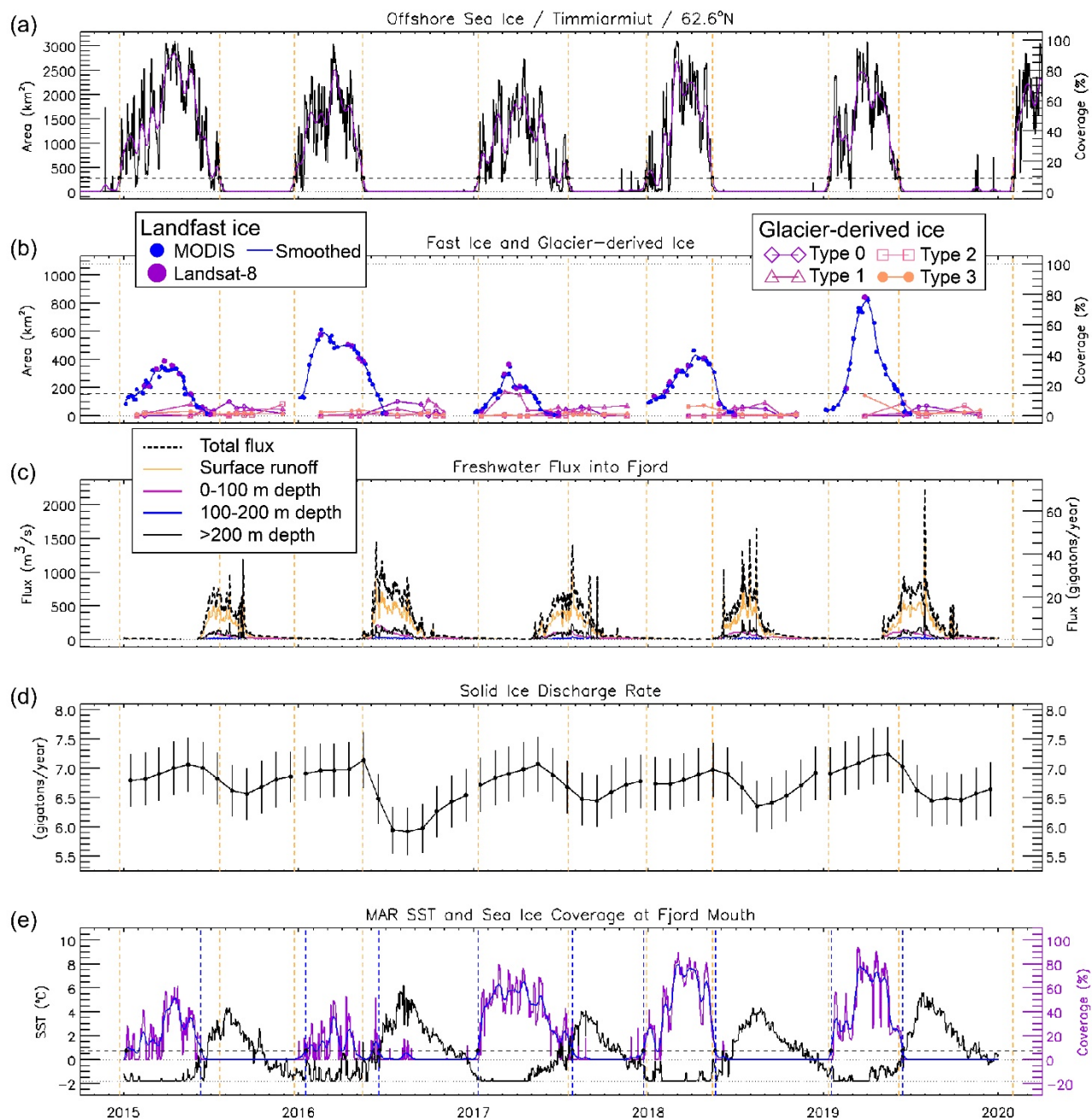
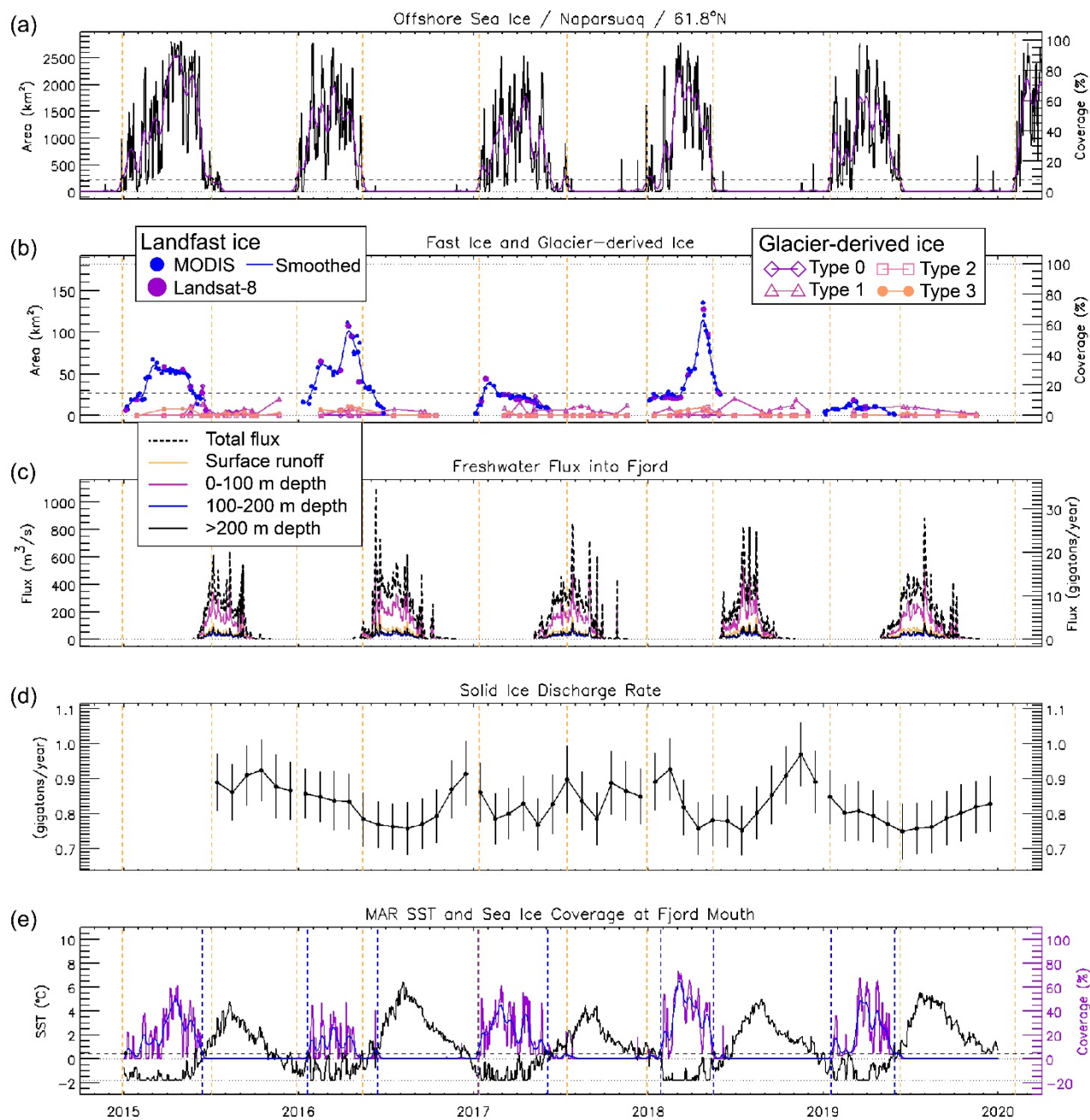


Figure A5. Same as Fig. A2 for fjord 40 (Timmarmiut).

413  
 414  
 415



416  
 417

Figure A6. Same as Fig. A2 for fjord 43 (Naparsuaq).

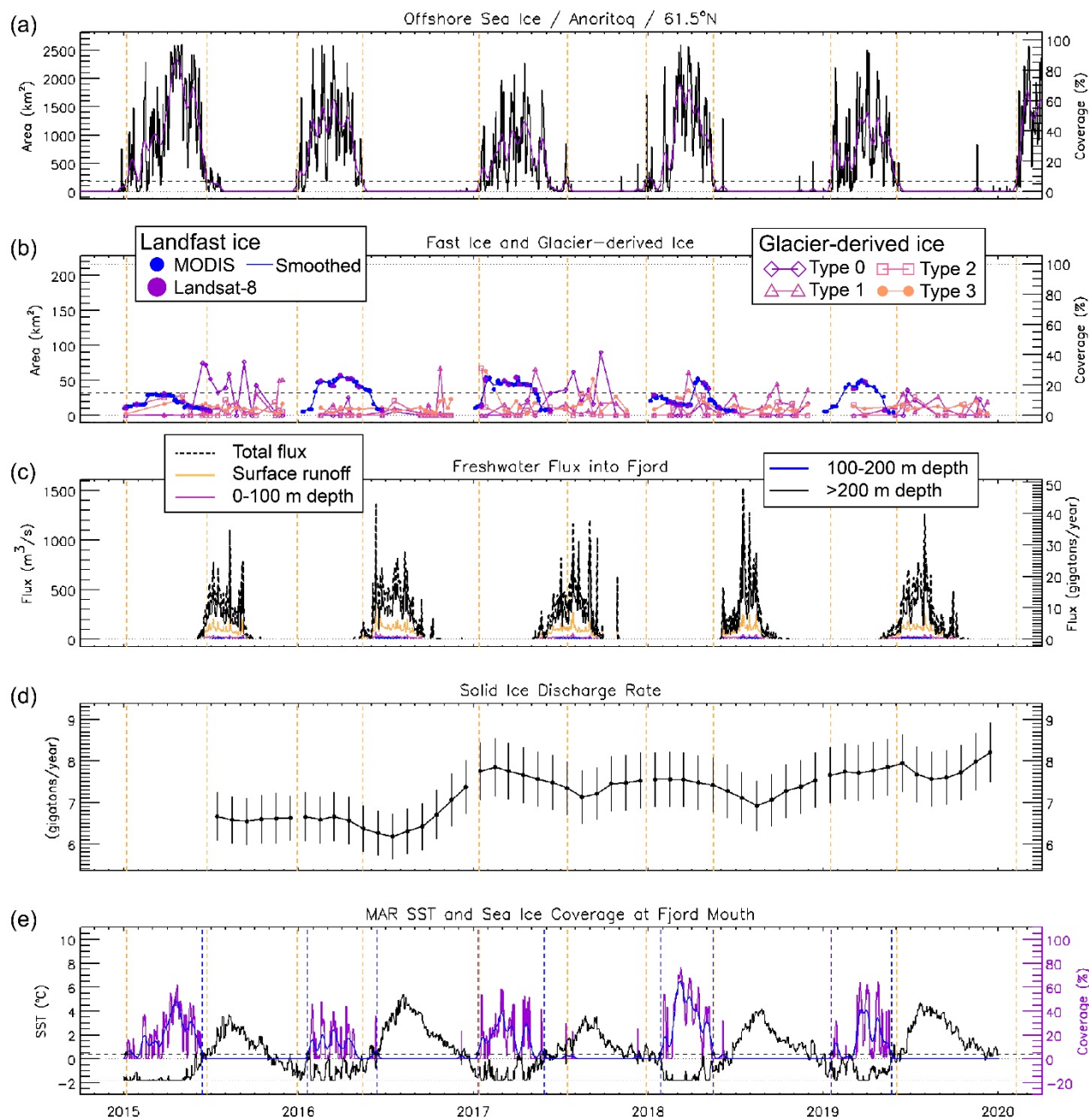
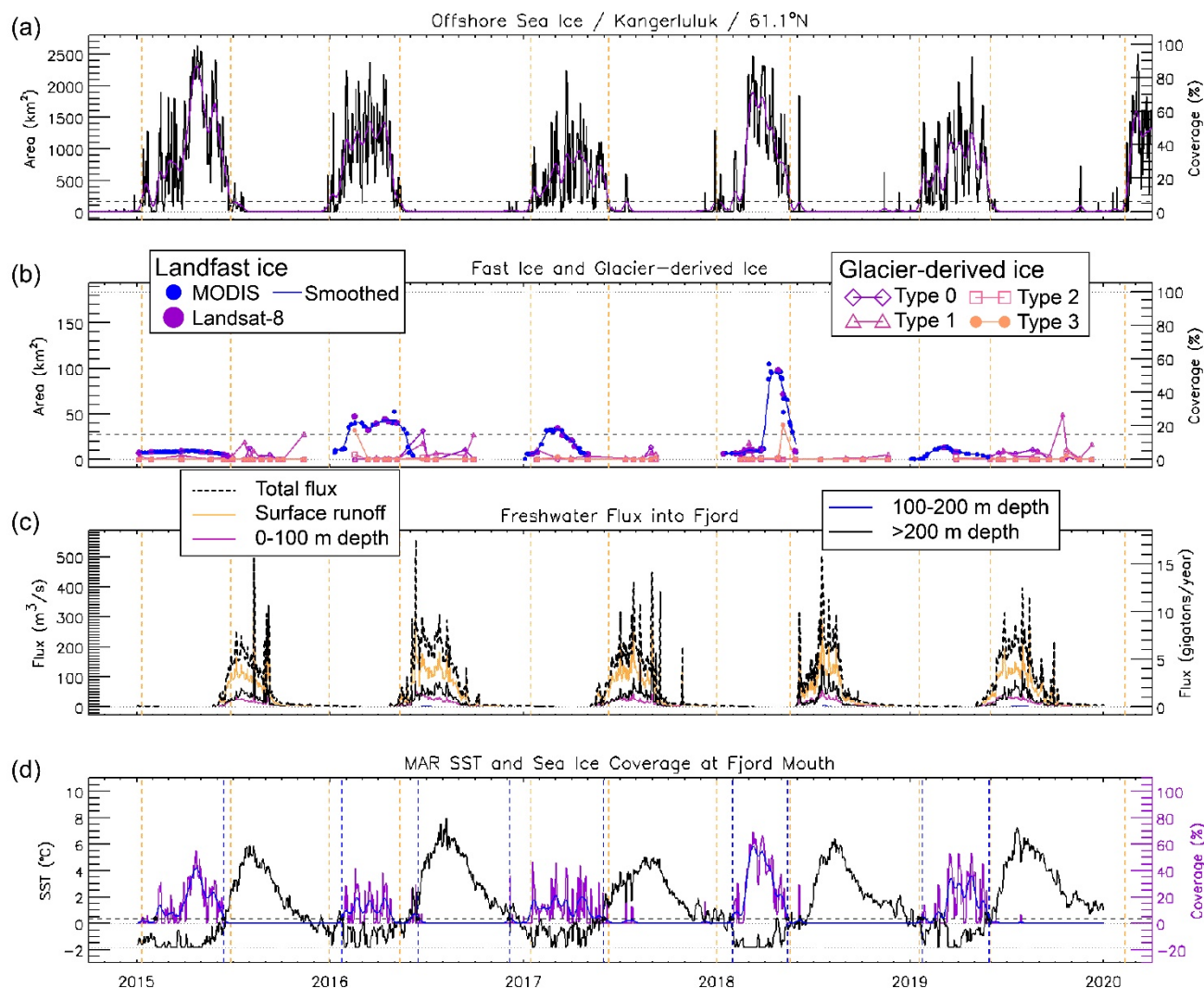


Figure A7. Same as Fig. A2 for fjord 45 (Anoritoq).

418  
419



420  
421 **Figure A8.** Same as Fig. A2 for fjord 48 (Kangerluluk), but with no solid ice discharge data and panel (e) presented as panel (d).

422  
423  
424  
425  
426  
427  
428  
429



430 **Table A1. Statistics for landfast ice in SEG focus fjords. Using a threshold of 15% areal coverage to define the landfast**  
 431 **ice season, each table entry contains the start day (day-of-year, doy), end day (doy), and duration (days) of the landfast**  
 432 **ice season. Landfast ice analysis did not span the full 12-month year and < symbol indicates likely earlier presence**  
 433 **while the > symbol indicates likely later/longer presence. Years when the landfast ice coverage never exceeded the 15%**  
 434 **threshold are marked as ---. The last two columns give the mean and standard deviation of the start day (doy), end day**  
 435 **(doy), and duration (days). Standard deviation is not calculated for records of likely longer length (> or < included).**  
 436 **Dates are based on use of smoothed data (see section 3.3).**

	2015	2016	2017	2018	2019	Mean	Stdv
<b>Nansen</b>	Start day (doy) <42	<34	<47	<65	<30	<43.6	
	End day (doy) >179	>159	175	148	144	>161.1	
	Duration (days) >137	>125	>128	>83	>114	>117.5	
<b>Kangerdlugssuaq</b>	<32	<35	<47	<34	<31	<35.8	
	>182	157	158	158	142	>159.3	
	>150	>122	>111	>124	>111	>123.4	
<b>Ikertivaq</b>	65	<31	34	50	<25	<40.8	
	160	124	137	119	116	131.1	18.0
	95	>93	103	69	>91	>90.2	
<b>Skjoldungen</b>	52	28	62	25	31	39.6	16.3
	148	163	124	148	120	140.4	18.3
	96	135	62	123	89	100.8	28.8
<b>Timmiarmiut</b>	30	11	52	35	43	34.0	15.5
	134	164	120	145	159	144.3	18.0
	104	153	68	110	116	110.3	30.4
<b>Naparsuaq</b>	43	27	22	70	---	40.3	21.6
	147	156	52	151	---	126.4	50.1
	104	129	30	81	---	86.1	42.2
<b>Anoritoq</b>	---	36	21	94	42	48.4	31.8
	---	148	130	127	117	130.4	13.3
	---	112	109	33	75	81.9	37.2
<b>Kangerluluk</b>	---	34	43	89	---	55.3	29.5
	---	143	76	144	---	120.8	39.0
	---	109	33	55	---	65.6	38.7

438 **Code and data availability**

439 Data created to support this research is archived at the National Snow and Ice Data Center (Cohen et al., 2023).

440 The code for freshwater and solid ice discharge data analysis and visualization is available at

441 [https://github.com/tarynblack/southeast\\_greenland\\_fjords](https://github.com/tarynblack/southeast_greenland_fjords) [This will be formally archived as a repository with DOI before  
 442 final publication].



443 Solid ice discharge data: v79 published 2023-05-05 at [https://doi.org/10.22008/promice/data/ice\\_discharge/d/v02](https://doi.org/10.22008/promice/data/ice_discharge/d/v02)

444 Freshwater discharge data: v4.2 published 2022-08-28 at <https://doi.org/10.22008/FK2/XKQVL7>

#### 445 **Author contributions and competing interests**

446 We used the CRediT taxonomy (<https://casrai.org/credit/>) to evaluate individuals' contributions and order authorship. All  
447 authors designed the study and contributed to the writing and editing of the manuscript. TM and KL administrated the project  
448 with TM supervising this research component. BC, TB, and HS were responsible for data collection and formal analyses. TM,  
449 BC, TB, and HS validated data and produced data visualizations. IJ advised regarding early research methods.  
450 The authors declare that they have no conflicts of interest.

#### 451 **Acknowledgements**

452 This research was supported via NASA Biological Diversity and Ecological Forecasting Programs and Cryospheric Sciences  
453 (NNX11AO63G, NNX13AN28G, and 80NSSC18K1229). We acknowledge Xavier Fettweis for assistance with MAR  
454 regional climate model data and Brice Noël for assistance with RACMO regional climate model data (included in some  
455 archived code and data but not within published results).

#### 456 **References [TO BE FORMATTED AFTER JOURNAL ACCEPTANCE]**

457 Aschwanden, A., Fahnestock, M. A., Truffer, M., Brinkerhoff, D. J., Hock, R., Khroulev, C., Mottram, R., and Khan, S. A.:  
458 Contribution of the Greenland Ice Sheet to sea level over the next millennium, 5, eaav9396,  
459 <https://doi.org/10.1126/sciadv.aav9396>, 2019.

460 Beitsch, A., L. Kaleschke, and S. Kern (2014). Investigating High-Resolution AMSR2 Sea Ice Concentrations during the  
461 February 2013 Fracture Event in the Beaufort Sea. *Remote Sensing*, 6, 3841-3856, doi:10.3390/rs6053841.  
462 <http://www.mdpi.com/2072-4292/6/5/3841>.

463 Bochow, N., Poltronieri, A., Robinson, A., Montoya, M., Rypdal, M., and Boers, N.: Overshooting the critical threshold for  
464 the Greenland ice sheet, *Nature*, 622, 528–536, <https://doi.org/10.1038/s41586-023-06503-9>, 2023.

465 Bosson, J. B., Huss, M., Cauvy-Fraunié, S., Clément, J. C., Costes, G., Fischer, M., Poulénard, J., and Arthaud, F.: Future  
466 emergence of new ecosystems caused by glacial retreat, *Nature*, 620, 562–569, <https://doi.org/10.1038/s41586-023-06302-2>,  
467 2023.



- 468 Cohen, B., T. Black, T. Moon. 2023. Southeast Greenland Fjord Physical Characteristics for 2015-2019. Boulder, Colorado  
469 USA. NASA National Snow and Ice Data Center Distributed Active Archive Center. [https://doi.org/](https://doi.org/10.5067/R86BW8LR6PZH)  
470 10.5067/R86BW8LR6PZH. (*Under Review*)
- 471 Fettweis, X., Box, J. E., Agosta, C., Amory, C., Kittel, C., Lang, C., As, D. V., Machguth, H., and Gallée, H.:  
472 Reconstructions of the 1900–2015 Greenland ice sheet surface mass balance using the regional climate MAR model, 11,  
473 1015–1033, <https://doi.org/10.5194/tc-11-1015-2017>, 2017.
- 474 Fox-Kemper, B., H.T. Hewitt, C. Xiao, G. Aðalgeirsdóttir, S.S. Drijfhout, T.L. Edwards, N.R. Golledge, M. Hemer,  
475 R.E. Kopp, G. Krinner, A. Mix, D. Notz, S. Nowicki, I.S. Nurhati, L. Ruiz, J.-B. Sallée, A.B.A. Slangen, and Y. Yu, 2021:  
476 Ocean, Cryosphere and Sea Level Change. In *Climate Change 2021: The Physical Science Basis. Contribution of Working*  
477 *Group I to the Sixth Assessment Report of the Intergovernmental Panel on Climate Change* [Masson-Delmotte, V., P. Zhai,  
478 A. Pirani, S.L. Connors, C. Péan, S. Berger, N. Caud, Y. Chen, L. Goldfarb, M.I. Gomis, M. Huang, K. Leitzell, E. Lonnoy,  
479 J.B.R. Matthews, T.K. Maycock, T. Waterfield, O. Yelekçi, R. Yu, and B. Zhou (eds.)]. Cambridge University Press,  
480 Cambridge, United Kingdom and New York, NY, USA, pp. 1211–1362, doi:10.1017/9781009157896.011.
- 481 Gallagher, M. R., Shupe, M. D., Chepfer, H., and L'Ecuyer, T.: Relating snowfall observations to Greenland ice sheet mass  
482 changes: an atmospheric circulation perspective, *Cryosphere*, 16, 435–450, <https://doi.org/10.5194/tc-16-435-2022>, 2021.
- 483 Gelderloos, R., T.W.N. Haine, and M. Almansi (2022). Subinertial variability in four Southeast Greenland fjords in realistic  
484 numerical simulations. *Journal of Geophysical Research: Oceans*, 127, e2022JC018820.  
485 <https://doi.org/10.1029/2022JC018820>.
- 486 Hawkings, J. R., Linhoff, B. S., Wadham, J. L., Stibal, M., Lamborg, C. H., Carling, G. T., Lamarche-Gagnon, G., Kohler,  
487 T. J., Ward, R., Hendry, K. R., Falteisek, L., Kellerman, A. M., Cameron, K. A., Hatton, J. E., Tingey, S., Holt, A. D.,  
488 Vinšová, P., Hofer, S., Bulínová, M., Větrovský, T., Meire, L., and Spencer, R. G. M.: Large subglacial source of mercury  
489 from the southwestern margin of the Greenland Ice Sheet, *Nat Geosci*, 14, 496–502, [https://doi.org/10.1038/s41561-021-](https://doi.org/10.1038/s41561-021-00753-w)  
490 00753-w, 2021.
- 491 Heide-Jørgensen, M. P., Chambault, P., Jansen, T., Gjelstrup, C. V. B., Rosing-Asvid, A., Macrander, A., Vikingsson, G.,  
492 Zhang, X., Andresen, C. S., and MacKenzie, B. R.: A regime shift in the Southeast Greenland marine ecosystem, *Global*  
493 *Change Biol*, <https://doi.org/10.1111/gcb.16494>, 2022.
- 494 Hersbach, H. *et al.* The ERA5 global reanalysis. *Q. J. R. Meteorol. Soc.* **146**, 1999–2049 (2020).
- 495 Hopwood, M. J., Carroll, D., Browning, T. J., Meire, L., Mortensen, J., Krisch, S., and Achterberg, E. P.: Non-linear  
496 response of summertime marine productivity to increased meltwater discharge around Greenland, 1–9,  
497 <https://doi.org/10.1038/s41467-018-05488-8>, 2018.



- 498 Hopwood, M. J., Carroll, D., Dunse, T., Hodson, A., Holding, J. M., Iriarte, J. L., Ribeiro, S., Achterberg, E. P., Cantoni, C.,  
499 Carlson, D. F., Chierici, M., Clarke, J. S., Cozzi, S., Fransson, A., Juul-Pedersen, T., Winding, M. H. S., and Meire, L.:  
500 Review article: How does glacier discharge affect marine biogeochemistry and primary production in the Arctic?, 14, 1347–  
501 1383, <https://doi.org/10.5194/tc-14-1347-2020>, 2020.
- 502 Kaleschke, L. and X. Tian-Kunze (2016). AMSR2 ASI 3.125 km Sea Ice Concentration Data, V0.1, Institute of Oceanography,  
503 University of Hamburg, Germany, digital media (<ftp-projects.zmaw.de/seoice/>).
- 504 Kelly, B. P., J. L. Bengtson, P. L. Boveng, M. F. Cameron, S. P. Dahle, J. K. Jansen, E. A. Logerwell, J. E. Overland, C. L.  
505 Sabine, G. T. Waring, and J. M. Wilder 2010. Status review of the ringed seal (*Phoca hispida*). U.S. Dep. Commer., NOAA  
506 Tech. Memo. NMFS-AFSC-212, 250 p.
- 507 Kim, Y.-H., Min, S.-K., Gillett, N. P., Notz, D., and Malinina, E.: Observationally-constrained projections of an ice-free  
508 Arctic even under a low emission scenario, *Nat. Commun.*, 14, 3139, <https://doi.org/10.1038/s41467-023-38511-8>, 2023.
- 509 Kochtitzky, W. & Copland, L. Retreat of Northern Hemisphere Marine-Terminating Glaciers, 2000–2020. *Geophys Res Lett*  
510 **49**, (2022).
- 511 Laidre, K. L. and I. Stirling. 2020. Grounded icebergs as maternity denning habitat for polar bears (*Ursus maritimus*) in  
512 North and Northeast Greenland. *Polar Biology* 43(7): 937-943, [10.1007/s00300-020-02695-2](https://doi.org/10.1007/s00300-020-02695-2).
- 513 Laidre, K. L., Supple, M. A., Born, E. W., Regehr, E. V., Wiig, Ø., Ugarte, F., Aars, J., Dietz, R., Sonne, C., Hegelund, P.,  
514 Isaksen, C., Akse, G. B., Cohen, B., Stern, H. L., Moon, T., Vollmers, C., Corbett-Detig, R., Paetkau, D., and Shapiro, B.:  
515 Glacial ice supports a distinct and undocumented polar bear subpopulation persisting in late 21st-century sea-ice conditions,  
516 *Science*, **376**, 1333–1338, <https://doi.org/10.1126/science.abk2793>, 2022.
- 517 Lenaerts, J. T. M., Medley, B., Broeke, M. R., and Wouters, B.: Observing and Modeling Ice Sheet Surface Mass Balance,  
518 *Reviews Of Geophysics*, 57, 376–420, <https://doi.org/10.1029/2018rg000622>, 2019.
- 519 Mahoney, A. R., Eicken, H., Gaylord, A. G., and Gens, R.: Landfast sea ice extent in the Chukchi and Beaufort Seas: The  
520 annual cycle and decadal variability, *Cold Reg Sci Technol*, 103, 41–56, <https://doi.org/10.1016/j.coldregions.2014.03.003>,  
521 2014.
- 522 Mankoff, K.: "Greenland freshwater runoff, GEUS Dataverse, V2, <https://doi.org/10.22008/FK2/AA6MTB>, 2020.
- 523 Mankoff, K. D., Noël, B., Fettweis, X., Ahlstrøm, A. P., Colgan, W., Kondo, K., Langley, K., Sugiyama, S., van As, D., and  
524 Fausto, R. S.: Greenland liquid water discharge from 1958 through 2019, *Earth Syst. Sci. Data*, 12, 2811–2841,  
525 <https://doi.org/10.5194/essd-12-2811-2020>, 2020a.
- 526 Mankoff, K. D.; Solgaard, A., Larsen, S.: Greenland Ice Sheet solid ice discharge from 1986 through last month: Discharge,  
527 GEUS Dataverse, V54, [https://doi.org/10.22008/promice/data/ice\\_discharge/d/v02](https://doi.org/10.22008/promice/data/ice_discharge/d/v02), 2020b.



- 528 Mankoff, K. D., Solgaard, A., Colgan, W., Ahlstrøm, A. P., Khan, S. A., and Fausto, R. S.: Greenland Ice Sheet solid ice  
529 discharge from 1986 through March 2020, *Earth Syst. Sci. Data*, 12, 1367–1383, <https://doi.org/10.5194/essd-12-1367-2020>,  
530 2020c.
- 531 McGovern, M., A. E. Poste, E. Oug, P. E. Renaud, H. C. Trannum. Riverine impacts on benthic biodiversity and functional  
532 traits: A comparison of two sub-Arctic fjords. *Estuarine, Coastal and Shelf Science* **240**, (2020),  
533 <https://doi.org/10.1016/j.ecss.2020.106774>.
- 534 Meire, L., Paulsen, M. L., Meire, P., Rysgaard, S., Hopwood, M. J., Sejr, M. K., Stuart-Lee, A., Sabbe, K., Stock, W., and  
535 Mortensen, J.: Glacier retreat alters downstream fjord ecosystem structure and function in Greenland, *Nat. Geosci.*, 16, 671–  
536 674, <https://doi.org/10.1038/s41561-023-01218-y>, 2023.
- 537 Moon, T. A., Gardner, A. S., Csatho, B., Parmuzin, I., and Fahnestock, M. A.: Rapid reconfiguration of the Greenland Ice  
538 Sheet coastal margin, 1–25, <https://doi.org/10.1029/2020jf005585>, 2020.
- 539 Moon, T. A., K. D. Mankoff, R. S. Fausto, X. Fettweis, B. D. Loomis, T. L. Mote, K. Poinar, M. Tedesco, A. Wehrlé, and C.  
540 D. Jensen, 2022: Greenland Ice Sheet. *Arctic Report Card 2022*, M. L. Druckenmiller, R. L. Thoman, and T. A. Moon, Eds.,  
541 <https://doi.org/10.25923/c430-hb50>.
- 542 Morlighem, M., C. Williams, E. Rignot, L. An, J. E. Arndt, J. Bamber, G. Catania, N. Chauché, J. A. Dowdeswell, B.  
543 Dorschel, I. Fenty, K. Hogan, I. Howat, A. Hubbard, M. Jakobsson, T. M. Jordan, K. K. Kjeldsen, R. Millan, L. Mayer, J.  
544 Mouginit, B. Noël, C. O’Cofaigh, S. J. Palmer, S. Rysgaard, H. Seroussi, M. J. Siegert, P. Slabon, F. Straneo, M. R. van den  
545 Broeke, W. Weinrebe, M. Wood, and K. Zinglensen. 2017. BedMachine v3: Complete bed topography and ocean bathymetry  
546 mapping of Greenland from multi-beam echo sounding combined with mass conservation. *Geophysical Research Letters*.  
547 44. DOI: 10.1002/2017GL074954.
- 548 Morlighem, M. et al. (2022). IceBridge BedMachine Greenland, Version 5 [Data Set]. Boulder, Colorado USA. NASA  
549 National Snow and Ice Data Center Distributed Active Archive Center. <https://doi.org/10.5067/GMEVBWFLWA7X>. Date  
550 [Accessed 11-02-2023](#).
- 551 Noël, B., Berg, W. J. van de, Science, S. L., 2019: Rapid ablation zone expansion amplifies north Greenland mass loss,  
552 2019.
- 553 Petrich, C., Eicken, H., Zhang, J., Krieger, J., Fukamachi, Y., and Ohshima, K. I.: Coastal landfast sea ice decay and breakup  
554 in northern Alaska: Key processes and seasonal prediction, *Journal of Geophysical Research*, 117, C02003,  
555 <https://doi.org/10.1029/2011jc007339>, 2012.
- 556 Rastner, P., Bolch, T., Mölg, N., Machguth, H., Bris, R. L., and Paul, F.: The first complete inventory of the local glaciers  
557 and ice caps on Greenland, *The Cryosphere*, 6, 1483–1495, <https://doi.org/10.5194/tc-6-1483-2012>, 2012.  
558



- 559 Scheick, J., Enderlin, E. M., and Hamilton, G.: Semi-automated open water iceberg detection from Landsat applied to Disko  
560 Bay, West Greenland, *Journal Of Glaciology*, 65, 468–480, <https://doi.org/10.1017/jog.2019.23>, 2019.
- 561 Soldal, I., Dierking, W., Korosov, A., and Marino, A.: Automatic Detection of Small Icebergs in Fast Ice Using Satellite  
562 Wide-Swath SAR Images, *Remote Sensing*, 11, 806–24, <https://doi.org/10.3390/rs11070806>, 2019.
- 563 Stern, H. L. and Laidre, K. L.: Sea-ice indicators of polar bear habitat, *The Cryosphere*, 10, 2027–2041,  
564 <https://doi.org/10.5194/tc-10-2027-2016>, 2016.
- 565 Dirk van As, Bent Hasholt, Andreas P. Ahlstrøm, Jason E. Box, John Cappelen, William Colgan, Robert S. Fausto, Sebastian  
566 H. Mernild, Andreas Bech Mikkelsen, Brice P.Y. Noël, Dorthe Petersen & Michiel R. van den Broeke (2018) Reconstructing  
567 Greenland Ice Sheet meltwater discharge through the Watson River (1949–2017), *Arctic, Antarctic, and Alpine*  
568 *Research*, 50:1, DOI: 10.1080/15230430.2018.1433799
- 569 van Dongen, E. C. H., Jouvét, G., Sugiyama, S., Podolskiy, E. A., Funk, M., Benn, D. I., Lindner, F., Bauder, A., Seguinot,  
570 J., Leinss, S., and Walter, F.: Thinning leads to calving-style changes at Bowdoin Glacier, Greenland, *The Cryosphere*, 15,  
571 485–500, <https://doi.org/10.5194/tc-15-485-2021>, 2021.
- 572 White, D.R. Propagation of Uncertainty and Comparison of Interpolation Schemes. *Int J Thermophys* 38, 39 (2017).  
573 <https://doi.org/10.1007/s10765-016-2174-6>